UNIVERSIDADE FEDERAL DE PERNAMBUCO
CENTRO DE CIÊNCIAS EXATAS E DA NATUREZA
PROGRAMA DE PÓS-GRADUAÇÃO EM FÍSICA

José Mário da Silva Filho

Numerical Determination of Local Models in Networks

Recife

2022

José Mário da Silva Filho

Numerical Determination of Local Models in Networks

Trabalho apresentado ao Programa de Pós-graduação em Física do Centro de Ciências Exatas e da Natureza da Universidade Federal de Pernambuco, como requisito parcial para obtenção do grau de Mestre em Física.

Área de Concentração: Física Teórica e Computacional

Orientador: Fernando Roberto de Luna Parisio Filho

Recife

2022

Catalogação na fonte
Bibliotecária Nataly Soares Leite Moro, CRB4-1722

S586n Silva Filho, José Mário da
Numerical determination of local models in networks / José Mário da Silva Filho. – 2022.
53 f.: il., fig., tab.

Orientador: Fernando Roberto de Luna Parisio Filho.
Dissertação (Mestrado) – Universidade Federal de Pernambuco. CCEN, Física, Recife, 2022.
Inclui referências.

1. Física teórica e computacional. 2. Não-localidade quântica em redes. 3. Modelos n-locais. 4. Não-localidade de Bell. I. Parisio Filho, Fernando Roberto de Luna (orientador). II. Título.

530.1 CDD (23. ed.) UFPE- CCEN 2022 - 94

JOSÉ MÁRIO DA SILVA FILHO

NUMERICAL DETERMINATION OF LOCAL MODELS IN NETWORKS

Dissertação apresentada ao Programa de Pós-Graduação em Física da Universidade Federal de Pernambuco, como requisito parcial para a obtenção do título de Mestre em Física.

Aprovada em: 13/05/2022.

BANCA EXAMINADORA

_____

Prof. Fernando Roberto de Luna Parisio Filho
Orientador
Universidade Federal de Pernambuco

_____

Profa. Nadja Kolb Bernardes
Examinadora Interna
Universidade Federal de Pernambuco

_____

Prof. Rafael Luiz da Silva Rabelo
Examinador Externo
Universidade Estadual de Campinas

AGRADECIMENTOS

A minha esposa Ana Paula, pelo seu apoio incondicional ao meu sonho de estudar Física.

A meu orientador Fernando Parisio, pelas enriquecedoras sugestões durante a elaboração do texto, e sobretudo por ter sido meu guia no aprendizado de Mecânica Quântica.

A minha mãe Maria Marluce, por me ensinar a ser perseverante perante dificuldades e a ter curiosidade sobre como funciona a Natureza.

A meu amigo Rafael Luz, pelas valiosas conversas sobre Física, Matemática e Python.

Quantum mechanics is certainly imposing. But an inner voice tells me that it is not yet the real thing. The theory says a lot, but does not really bring us any closer to the secret of the 'old one'. I, at any rate, am convinced that *He* is not playing at dice. (EINSTEIN et al., 1971).

ABSTRACT

Taking advantage of the fact that the cardinalities of hidden variables in network scenarios can be taken to be finite without loss of generality, a numerical tool for finding explicit local models that reproduce a given statistical behaviour was developed. The numerical procedure was then applied to get numerical estimates to two interesting problems in the context of network non-locality: i) for which critical visibility the Greenberger-Horne-Zeilinger (GHZ) distribution ceases to be local in the triangle scenario with no inputs; ii) what is the boundary of the local set in a given 2-dimensional slice of the probability space for the bilocal network with binary inputs and outputs. For the first problem: a critical visibility of $v \approx 1/3$ was found; behaviours with $v \leq 1/3$ were proven to be trilocal; and numerical evidence that behaviours with $v > 1/3$ are not trilocal was found. For the second problem: a closed set that approximates the bilocal set was found; behaviours inside this set were proven to be bilocal; and numerical evidence that behaviours outside this set are not bilocal was found.

Keywords: quantum network nonlocality; n-local models; Bell nonlocality.

RESUMO

Valendo-se do fato de que as cardinalidades de variáveis ocultas em cenários de rede podem ser assumidas finitas sem perda de generalidade, foi desenvolvida uma ferramenta numérica para encontrar modelos locais explícitos que reproduzem um comportamento estatístico dado. O procedimento numérico foi então utilizado para obter estimativas numéricas para dois problemas interessantes no contexto de não-localidade em redes: i) para qual visibilidade crítica a distribuição Greenberger-Horne-Zeilinger (GHZ) deixa de ser local no cenário triangular sem inputs; ii) qual a fronteira do conjunto local em uma dada secção bidimensional do espaço de probabilidades para a rede bilocal com inputs e outputs binários. Para o primeiro problema: encontrou-se uma visibilidade crítica de $v \approx 1/3$; provou-se que comportamentos com $v \leq 1/3$ são trilocais; e encontrou-se evidência numérica de que comportamentos com $v > 1/3$ não são trilocais. Para o segundo problema: encontrou-se um conjunto fechado que aproxima o conjunto bilocal; provou-se que comportamentos no interior desse conjunto são bilocais; e encontrou-se evidência numérica de que comportamentos no exterior desse conjunto não são bilocais.

Palavras-chaves: não-localidade quântica em redes; modelos n-locais; não-localidade de Bell.

LISTA DE FIGURAS

LISTA DE TABELAS

SUMÁRIO

1 INTRODUCTION

Randomness is at the heart of quantum mechanics. It does not take much time in the study of quantum theory to realize that probabilities play a central role. Take for example a two level system (such as the spin of an electron) in the state

$$|\psi\rangle = \frac{1}{\sqrt{2}} \left(|0\rangle + |1\rangle \right). \tag{1.1}$$

Consider also the observable

$$\sigma_z = |0\rangle \langle 0| - |1\rangle \langle 1|. \tag{1.2}$$

Every physicist knows that by measuring σ_z in state $|\psi\rangle$, the result is either $+1$ or -1 with equal probabilities of $1/2$. Say we get the result $+1$. Are we then allowed to conclude that this information was somehow encoded in the system before the measurement and we were simply ignorant of this? Or is the description of equation 1.1 complete, in the sense that it encapsulates all that can be known about the system before measurement? In other words, are there perhaps some hidden variables that, if known, could allow us to predict with certainty the outcome of the measurement? Or is nature random in a fundamental level?

Questions such as these led to much discussion among the scientists who were trying to put quantum mechanics together in the 1920s (BAGGOTT, 2004). Two prominent figures of this period were physicists Albert Einstein and Niels Bohr. They took radically different stances regarding the interpretation of the newly discovered quantum theory, and their exchanges on the subject became known as the Einstein-Bohr debates. Einstein had a philosophical conviction that nature does not "play dice", as stated by him in a 1926 letter to Max Born[1]. Bohr, on the other hand, embraced the intrinsic probabilistic character of the theory.

In 1935, Einstein and colleagues Boris Podolsky and Nathan Rosen wrote a paper titled "Can Quantum-Mechanical Description of Physical Reality Be Considered Complete?", in which the authors present a thought experiment designed to prove that quantum mechanics was not a complete theory (EINSTEIN; PODOLSKY; ROSEN, 1935). This counterargument became to be known as the Einstein-Podolsky-Rosen (EPR) paradox, and would eventually inspire physicist John Stewart Bell to discover quantum non-locality some 30 years later (BELL, 1964). It is rather interesting that such an important feature of quantum mechanics owes its discovery to an argument designed to expose an alleged imperfection of the theory.

[1] Einstein's famous quote is the epigraph of this dissertation.

The EPR paradox relies on yet another peculiar characteristic of quantum mechanics: entanglement. In systems with more than one degree of freedom, it is possible to conceive of wavefunctions with a correlation between different parts of the system. Take for example a composite system consisting of a pair of two level systems (such as the spins of two electrons) in the state

$$|\psi\rangle = \frac{1}{\sqrt{2}} \left(|01\rangle - |10\rangle \right). \tag{1.3}$$

In such a state, the spins of the two electrons are said to be entangled. As soon as we measure the spin of one particle in a given orientation, the wavefunction of the whole system collapses and we can be sure that a measurement of the spin of the other particle in that same orientation will yield the opposite result. This perfect negative correlation can in principle persist even if the two particles are spatially separated. EPR then proposed[2] the following argument with 3 premises: if i) we can choose to measure different observables (possibly non-commuting) in one particle, ii) each choice results in the other particle being described by different wavefunctions, and iii) measurements in one particle cannot bring about any real change in the other since they are spatially separated; then the wavefunction is an incomplete description of reality.

The most obvious way of fixing this alleged incompleteness in the theory would be to assume the existence of local hidden variables that could explain the correlations in entanglement experiments. This was done by Bell in his seminal paper (BELL, 1964), where he demonstrated that, under the tacit assumption that the choice of measurements can be made independently of the measured system, quantum mechanics makes experimental predictions which are incompatible with any local hidden variable theory. This incompatibility result is now known as Bell's theorem, and the irreconcilable aspect of quantum mechanics is now known as non-locality.

Bell's main contribution was to take an issue that was thought to be purely philosophical up until then and bring it down to the experimental level. In the following years, several experiments were performed to test local hidden variables and the predictions of quantum mechanics were consistently observed (FREEDMAN; CLAUSER, 1972) (ASPECT; DALIBARD; ROGER, 1982) (HENSEN et al., 2015) (SHALM et al., 2015) (GIUSTINA et al., 2015). The experiments increased in complexity along the decades in order to close loopholes that could still allow for some local hidden variable explanation. There are some loopholes that may never be completely closed, such as the measurement independence assumption, but given the experimental evidence

[2] In the original EPR paper, the authors considered a composite system with continuous degrees of freedom. The version of the argument presented here is due to (BOHM, 1951) and relies instead on discrete degrees of freedom, but the essence of the argument remains the same.

available today, I am of the opinion that it is no longer possible to reject non-locality in a consistent manner, without subscribing to even stranger hypotheses about nature.

The impact of non-locality is not restricted to the foundations of quantum mechanics though. The concept has found applications also in quantum information protocols to detect eavesdropping when sharing cryptographic keys (EKERT, 1991) and more generally for device-independent certification (ŠUPIĆ; BOWLES, 2020).

One important theoretical development is the notion of non-locality in networks, first introduced in (BRANCIARD; GISIN; PIRONIO, 2010). In standard Bell non-locality, there is only one source that distributes quantum states to two or more parties. In network non-locality, there are multiple independent sources that distribute quantum states to some parties, but not all of them. The introduction of network scenarios led to new forms of non-locality that are not yet fully understood. This dissertation aims to present a numerical tool that can be used to investigate the challenging subject of network non-locality.

In chapter 2, the concepts of standard Bell non-locality as well as network non-locality are explored in more detail. In chapter 3, the numerical tool is explained and then applied to two interesting problems regarding network non-locality. Finally, in chapter 4, the concluding remarks are presented, as well as some perspectives for future work expanding the ideas discussed in this dissertation.

2 NON-LOCALITY

First let us a define what is a Bell scenario. The situation closely resembles that of the EPR thought experiment (EINSTEIN; PODOLSKY; ROSEN, 1935) as formulated by (BOHM, 1951), the only differences being a more modern notation, following references (BRUNNER et al., 2014) and (SCARANI, 2019). Consider an experiment with two parties, Alice and Bob (see figure 1). They both perform measurements in subsystems that might have interacted in the past[1] (the asterisk sign in the figure). In her laboratory, Alice has a choice of measurements she can perform. Her chosen measurement setting will be denoted by x, and the output of her measurement device will be denoted by a. In the usual terminology of the field, x and a are called Alice's input and output, respectively. Likewise, on Bob's side, his input is denoted by y and his output is denoted by b. In the figures of this text, inputs will be represented by blue squares and outputs will be represented by green circles.

Figure 1 – Bipartite Bell scenario. The outputs of each party a and b are represented by green circles, while the inputs x and y are represented by blue squares (also known as measurement settings). The asterisk sign represents some system shared between the parties.

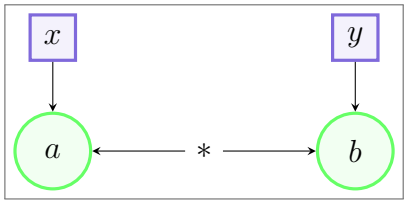

Source: personal archive

The statistical behaviour of the measurements performed by Alice and Bob can be characterized by the probability distribution $p(a, b|x, y)$. Frequently the words correlation and behaviour are also used to denote this probability distribution. In order to keep the notation uncluttered, I will not use subscripts to indicate probability distributions of different random variables. This will be done with the arguments of the distribution. For example, instead of writing $p_{AB}(a, b)$ or $p_A(a)$, I simply write $p(a, b)$ or $p(a)$.

Additionally, let us restrict ourselves to the case of a finite number of inputs and outputs, i.e.

[1] For now, the details of this composite system are not important. It could be a classical system, such as a string of correlated bits that is sent to each party, or a quantum one, such as a pair of entangled photons. As we shall briefly see, the latter system is fundamentally different from the former, due to the non-local character of quantum theory.

$$x \in \{1, 2, \ldots, M_A\}\,, \tag{2.1}$$

$$y \in \{1, 2, \ldots, M_B\}\,, \tag{2.2}$$

$$a \in \{1, 2, \ldots, m_A\}\,, \tag{2.3}$$

$$b \in \{1, 2, \ldots, m_A\}\,. \tag{2.4}$$

Hence, Alice has M_A possible measurement settings and m_A possible outputs for each measurement, while Bob has M_B possible measurement settings and m_B possible outputs for each measurement. The number of elements in a set is called cardinality, so we refer to M_A and M_B as the input cardinalities e to m_A and m_B as the output cardinalities.

A priori, the only conditions that must be required of the probabilities $p(a, b|x, y)$ are the positivity constraints and the normalization condition:

$$p(a, b|x, y) \geq 0, \qquad \forall a, b, x, y, \tag{2.5}$$

$$\sum_{a,b} p(a, b|x, y) = 1, \qquad \forall x, y. \tag{2.6}$$

A stronger condition that can be enforced over the behaviour $p(a, b|x, y)$ is that there is no way for one party to communicate her or his choice of input to the other party[2]. More precisely, the marginal distribution of Alice's output $p(a|x, y) = \sum_b p(a, b|x, y)$ is independent of the input chosen by Bob, and vice-versa. Mathematically, this can be expressed as the no-signalling constraints:

$$p(a|x, y) = p(a|x, y'), \qquad \forall x, y, y', \tag{2.7}$$

$$p(b|x, y) = p(b|x', y), \qquad \forall x, x', y. \tag{2.8}$$

This allows us to speak of marginal distributions $p(a|x)$ and $p(b|y)$ by removing the irrelevant input for the specific marginal. The set of behaviours that satisfy 2.7 and 2.8 is called the no-signalling set, represented by $\mathcal{NS}$.

A further restriction on the correlations shared by Alice and Bob is that the probability distribution $p(a, b|x, y)$ can be obtained by a quantum experiment. The most general way of expressing this condition is not with the projective measurements that are first presented in quantum mechanics textbooks but rather with POVM[3] measurements (NIELSEN; CHUANG,

[2] If the measurements of Alice and Bob are space-like separated events, this condition prevents faster than light communication, which would be at odds with special relativity.

[3] Postive operator-valued measure.

2000). This is further justified by the fact that we are only interested in the statistics of Alice and Bob measurements, characterized by the distribution $p(a,b|x,y)$. In this formalism, the POVM is a collection of operators $\{\Pi_i\}$ satisfying the following conditions:

$$\Pi_i \geq 0, \qquad \forall i, \tag{2.9}$$

$$\sum_i \Pi_i = I. \tag{2.10}$$

Each POVM element Π_i corresponds to a different measurement outcome. The probability p_i of the i-th outcome when measuring a system in a state represented by the density operator ρ is given by

$$p_i = \mathrm{Tr}\left(\rho\Pi_i\right). \tag{2.11}$$

Notice that unlike the usual projective measurements, the number of possible outcomes can be greater than the dimension of the system Hilbert space. Applying the POVM formalism to the Bell scenario, the behaviour $p(a,b|x,y)$ can be obtained by a quantum experiment if there are a quantum state ρ and POVMs $\{\Pi_a^x\}$ and $\{\Pi_b^y\}$ such that:

$$\Pi_a^x \geq 0, \qquad \forall a,x, \tag{2.12}$$

$$\Pi_b^y \geq 0, \qquad \forall b,y, \tag{2.13}$$

$$\sum_a \Pi_a^x = I_A, \qquad \forall x, \tag{2.14}$$

$$\sum_b \Pi_b^y = I_B, \qquad \forall y, \tag{2.15}$$

$$p(a,b|x,y) = \mathrm{Tr}\left[\rho\left(\Pi_a^x \otimes \Pi_b^y\right)\right]. \tag{2.16}$$

The superscript in the POVM elements denotes the measurement settings chosen by Alice and Bob, while the subscript denotes the measurement outcome. So there are M_A families of operators $\{\Pi_a^x\}$ for Alice, each with m_A outcomes, and analogously for Bob. The set of behaviours that could be represented by equation 2.16 is called the quantum set, represented by $\mathcal{Q}$. Notice that no restriction is placed on the Hilbert space in which the state ρ and the POVM elements operate. If there is one state ρ and POVMs $\{\Pi_a^x\}$, $\{\Pi_b^y\}$ that reproduce the probability distribution via equation 2.16, no matter how complicated they may be, the behaviour belongs to quantum set $\mathcal{Q}$.

Finally, it can be required that the behaviour $p(a,b|x,y)$ could be obtained by a process in which Alice and Bob share a local hidden variable, represented by λ (see figure 2). In the figures of this text, local hidden variables will be represented by red triangles, with arrows

denoting the parties with access to the hidden variable, which is sometimes referred to as shared randomness in the literature.

Figure 2 – Local bipartite Bell scenario. The outputs of each party a and b are represented by green circles, while the inputs x and y are represented by blue squares (also known as measurement settings). The local hidden variable λ shared between the parties is represented by a red triangle. A local behaviour $p(a, b|x, y)$ in such a scenario can always be cast into the form of equation 2.17.

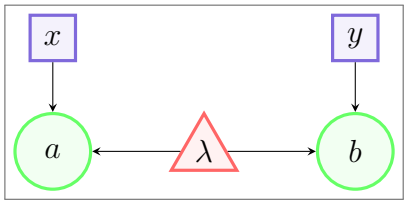

Source: personal archive

In this local Bell scenario, the hidden variable is a random variable distributed as $p(\lambda)$, and for a given value of λ and the inputs x, y, Alice and Bob subsystems determine locally the outputs according to the probability distributions $p(a|x, \lambda)$ and $p(b|y, \lambda)$, usually called the response functions of Alice and Bob. Putting all this together, the probability distribution $p(a, b|x, y)$ is given by

$$p(a, b|x, y) = \int d\lambda\, p(\lambda)p(a|x, \lambda)p(b|y, \lambda). \tag{2.17}$$

Notice that there is no requirement that the response functions $p(a|x, \lambda)$ and $p(b|y, \lambda)$ are deterministic. The set of behaviours that can be written as equation 2.17 is called the local set, represented by $\mathcal{L}$.

2.1 COLLINS-GISIN REPRESENTATION

Given a bipartite Bell scenario with input and output cardinalities given by M_A, M_B, m_A, m_B, there are $M_A M_B m_A m_B$ probabilities $p(a, b|x, y)$. However, because of the normalization conditions 2.6, only $m_A m_B - 1$ probabilities must be given for each pair of inputs (x, y) in order to specify the behaviour. Hence, the dimension of the full behaviour space is

$$D = M_A M_B (m_A m_B - 1). \tag{2.18}$$

In the case of no-signalling behaviours, the conditions 2.7 and 2.8 put additional constraints in the probabilities $p(a, b|x, y)$. Consider for example the simplest non trivial Bell scenario with $M_A = M_B = m_A = m_B = 2$. By setting the 4 marginal probabilities $p(a = 1|x = 1)$,

$p(a=1|x=2)$, $p(b=1|y=1)$ and $p(b=1|y=2)$, all the other marginal probabilities can be determined by the normalization constraints:

$$p(a=1|x=1)+p(a=2|x=1)=1, \tag{2.19}$$

$$p(a=1|x=2)+p(a=2|x=2)=1, \tag{2.20}$$

$$p(b=1|y=1)+p(b=2|y=1)=1, \tag{2.21}$$

$$p(b=1|y=1)+p(b=2|y=1)=1. \tag{2.22}$$

Next, for each input pair (x,y), only one joint probability, say, $p(ab=11|x,y)$ needs to be specified, because all the others can be determined by the following constraints:

$$p(ab=11|x,y)+p(ab=12|x,y)=p(a=1|x), \tag{2.23}$$

$$p(ab=11|x,y)+p(ab=21|x,y)=p(b=1|y), \tag{2.24}$$

$$\sum_{a,b\in\{1,2\}} p(a,b|x,y)=1. \tag{2.25}$$

The no signalling behaviour is therefore fully specified by the eight probabilities shown in the representation below:

$$p_{\mathcal{NS}}(a,b|x,y)\leftrightarrow \begin{array}{c|c|c} & p(a=1|x=1) & p(a=1|x=2) \\ \hline p(b=1|y=1) & p(ab=11|xy=11) & p(ab=11|xy=21) \\ \hline p(b=1|y=2) & p(ab=11|xy=12) & p(ab=11|xy=22) \end{array}. \tag{2.26}$$

The parametrization 2.26 is called the Collins-Gisin representation (COLLINS; GISIN, 2004)(SCARANI, 2019). By using the Collins-Gisin representation, the dimension of the no-signalling set $\mathcal{NS}$ for the general bipartite scenario can be found. First, set $M_A(m_A-1)$ marginals $p(a|x)$ for Alice and $M_B(m_B-1)$ marginals $p(b|y)$ for Bob. Now, for a specific pair of inputs (x,y), one has to specify $(m_A-1)(m_B-1)$ probabilities. Hence the dimension of the no-signalling set $\mathcal{NS}$ is

$$D_{\mathcal{NS}}=M_A(m_A-1)+M_B(m_B-1)+M_AM_B(m_A-1)(m_B-1).$$

$$D_{\mathcal{NS}}=[M_A(m_A-1)+1]\,[M_B(m_B-1)+1]-1. \tag{2.27}$$

The same process can be done for the multipartite case. Consider for example the scenario with 3 parties depicted in figure 3.

Figure 3 – Tripartite Bell scenario. The outputs of each party a, b and c are represented by green circles, while the inputs x, y and z are represented by blue squares (also known as measurement settings). The asterisk sign represents some system shared between the parties.

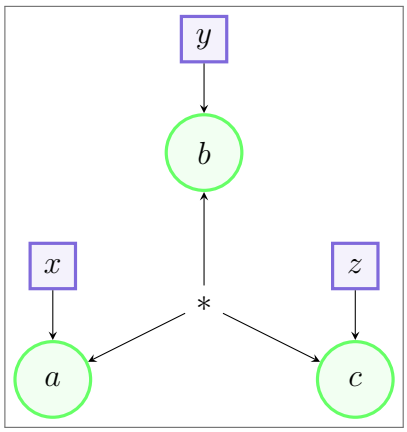

Source: personal archive

In order to specify a no-signalling distribution $p(a,b,c|x,y,z)$, we first set the marginals $p(a|x)$, $p(b|y)$ and $p(c|z)$ by providing $M_A(m_A-1)+M_B(m_B-1)+M_C(m_C-1)$ probabilities. Next, the bipartite marginals $p(a,b|x,y)$, $p(a,c|x,z)$ and $p(b,c|y,z)$ are specified by setting $M_AM_B(m_A-1)(m_B-1)+M_AM_C(m_A-1)(m_C-1)+M_BM_C(m_B-1)(m_C-1)$ probabilities. Finally the complete distribution $p(a,b,c|x,y,z)$ is specified by setting the remaining $M_AM_BM_C(m_A-1)(m_B-1)(m_C-1)$ probabilities. Hence, the dimension of the no-signalling set in the tripartite case is

$$\begin{aligned} D_{\mathcal{NS}} = {} & M_A(m_A-1)+M_B(m_B-1)+M_C(m_C-1)+M_AM_B(m_A-1)(m_B-1) \\ & + M_AM_C(m_A-1)(m_C-1)+M_BM_C(m_B-1)(m_C-1) \\ & + M_AM_BM_C(m_A-1)(m_B-1)(m_C-1). \end{aligned}$$

$$D_{\mathcal{NS}} = [M_A(m_A-1)+1]\,[M_B(m_B-1)+1]\,[M_C(m_C-1)+1]-1. \tag{2.28}$$

In a general Bell scenario with N parties, the dimension of the no-signalling set is given by

$$D_{\mathcal{NS}} = \prod_{i=1}^{N}\left[M_i\,(m_i-1)+1\right]-1, \tag{2.29}$$

do where M_i and m_i are the input and output cardinalities of the i-th party (ROSSET; GISIN; WOLFE, 2017).

2.2 THE LOCAL POLYTOPE

As previously mentioned, in a local model (equation 2.17) there is no restriction that the response functions $p(a|x,\lambda)$ and $p(b|y,\lambda)$ must be deterministic. However, as was shown in (FINE, 1982), it is the case that any local randomness used locally by Alice and Bob can be transferred to the hidden variable, so that the distribution $p(a,b|x,y)$ can be written as a convex combination of deterministic behaviours of the form

$$p_i(a,b|x,y) = \delta_{a,f_i(x)}\delta_{b,g_i(y)}. \tag{2.30}$$

Such behaviours are characterized by the deterministic output functions $a = f_i(x)$ and $b = g_i(y)$ for Alice and Bob. The following derivation of Fine's theorem is inspired by the argument of more modern references such as (BRUNNER et al., 2014) and (SCARANI, 2019), but with a slight modification that will serve us best in section 3.1.

Theorem 1. *(Fine) A local behaviour $p(a,b|x,y)$ can always be expressed as a convex combination of deterministic behaviours, i.e.*

$$p(a,b|x,y) = \sum_i q_i \delta_{a,f_i(x)}\delta_{b,g_i(y)}, \tag{2.31}$$

with $q_i \in [0,1]$ and $\sum_i q_i = 1$.

Proof. The behaviour $p(a,b|x,y)$ is local, so by definition (equation 2.17),

$$p(a,b|x,y) = \int d\lambda\, p(\lambda)p(a|x,\lambda)p(b|y,\lambda). \tag{2.32}$$

Let us construct a new local model with an expanded hidden variable $\lambda' = (\lambda,\mu,\nu)$. In this new model, $\mu = (\mu_1,\ldots,\mu_{M_A})$ is a discrete random variable that provides to Alice a deterministic response function mimicking the statistical behaviour of her original response function $p(a|x,\lambda)$. Likewise $\nu = (\nu_1,\ldots,\nu_{M_B})$ is a discrete random variable that provides to Bob a deterministic response function mimicking the statistical behaviour of his original response function $p(b|y,\lambda)$. In terms of the original local model (distributions represented by

$p(\cdot)$), the probability distributions that characterize the new model (represented by $p'(\cdot)$) are

$$p'(\lambda,\mu,\nu) = p(\lambda)p(\mu,\nu|\lambda) = p(\lambda)p'(\mu|\lambda)p'(\nu|\lambda), \tag{2.33}$$

$$p'(\mu|\lambda) = p(a=\mu_1|x=1,\lambda)\cdots p(a=\mu_{M_A}|x=M_A,\lambda) = \prod_{i=1}^{M_A} p(a=\mu_i|x=i,\lambda), \tag{2.34}$$

$$p'(\nu|\lambda) = p(b=\nu_1|y=1,\lambda)\cdots p(b=\nu_{M_B}|y=M_B,\lambda) = \prod_{j=1}^{M_B} p(b=\nu_j|y=j,\lambda), \tag{2.35}$$

$$p'(a|x,\lambda,\mu,\nu) = \delta_{a,\mu_x}, \tag{2.36}$$

$$p'(b|y,\lambda,\mu,\nu) = \delta_{b,\nu_y}. \tag{2.37}$$

This newly constructed model gives rise to the following behaviour:

$$\begin{aligned} p'(a,b|x,y) &= \int d\lambda \sum_{\mu,\nu} p'(\lambda,\mu,\nu)p'(a|x,\lambda,\mu,\nu)p'(b|y,\lambda,\mu,\nu) \\ &= \int d\lambda \sum_{\mu,\nu} p(\lambda) \prod_{i=1}^{M_A} p(a=\mu_i|x=i,\lambda) \prod_{j=1}^{M_B} p(b=\nu_j|y=j,\lambda)\delta_{a,\mu_x}\delta_{b,\nu_y} \\ &= \int d\lambda\, p(\lambda)p(a|x,\lambda)p(b|y,\lambda) \\ &= p(a,b|x,y). \end{aligned} \tag{2.38}$$

Notice this new model reproduces the original one. Also, it can be written as a convex combination of deterministic behaviours indexed by (μ,ν):

$$\begin{aligned} p'(a,b|x,y) &= \sum_{\mu,\nu} \left[\int d\lambda\, p(\lambda) \prod_{i=1}^{M_A} p(a=\mu_i|x=i,\lambda) \prod_{j=1}^{M_B} p(b=\nu_j|y=j,\lambda) \right] \delta_{a,\mu_x}\delta_{b,\nu_y} \\ &= \sum_{\mu,\nu} q_{\mu,\nu}\delta_{a,\mu_x}\delta_{b,\nu_y}, \end{aligned} \tag{2.39}$$

with weights $q_{\mu,\nu}$ given by

$$q_{\mu,\nu} = \int d\lambda\, p(\lambda) \prod_{i=1}^{M_A} p(a=\mu_i|x=i,\lambda) \prod_{j=1}^{M_B} p(b=\nu_j|y=j,\lambda). \tag{2.40}$$

This concludes the proof of Fine's theorem. □

A few remarks are in order. First, since any local behaviour can be written as a convex combination of the deterministic strategies, it follows that $\mathcal{L}$ is a convex set. Second, notice that the number of deterministic strategies is finite ($m_A^{M_A} m_B^{M_B}$), so $\mathcal{L}$ is the convex hull of a finite number of behaviours, therefore it is a polytope. Third and lastly, since $\mathcal{L}$ is a polytope,

it can be represented as the intersection of finitely many closed halfspaces (ZIEGLER, 2012). Each of these halfspaces is described by a linear inequality in the probabilities $p(a,b|x,y)$, with coefficients $s^i_{a,b,x,y}$ and a number S^i as the upper bound for the linear combination of the probabilities:

$$\sum_{a,b,x,y} s^i_{a,b,x,y} p(a,b|x,y) \leq S^i, \tag{2.41}$$

where the superscript i indexes the number of halfspaces that constitute the local polytope. The conditions 2.41 represent the facets of the local polytope and are called tight Bell inequalities. Tightness is used here in the sense that the facet inequalities bound the local set without any slack, i.e. they form a minimal family of necessary and sufficient conditions for a behaviour to be local. The violation of any of these expressions by a specific distribution $p(a,b|x,y)$ is said to witness the non-locality of the behaviour.

As a final note in this section, I would like to point out that in the proof of Fine's theorem presented above, the original hidden variable λ was extended to (λ,μ,ν) but the response function of Alice (respectively Bob) only takes μ (respectively ν) into account. So instead of distributing (λ,μ,ν) to both parties, we could just as well have distributed only (μ,ν). Therefore, when talking about local behaviours, not only can we assume without loss of generality that the response functions of Alice and Bob are deterministic, we can also assume that the hidden variable can take on a finite number of values, namely the number of deterministic strategies, $m_A^{M_A} m_B^{M_B}$. If we wanted only Alice's response function to be deterministic, we could have proposed the alternative model:

$$p'(\mu) = \int d\lambda\, p'(\lambda) p(\mu|\lambda) = \int d\lambda\, p(\lambda) \prod_{i=1}^{M_A} p(a=\mu_i|x=i,\lambda), \tag{2.42}$$

$$p'(a|x,\mu) = \delta_{a,\mu_x}, \tag{2.43}$$

$$p'(b|y,\mu) = \frac{\int d\lambda\, p(\lambda) \prod_{i=1}^{M_A} p(a=\mu_i|x=i,\lambda) p(b|y,\lambda)}{\int d\lambda\, p(\lambda) \prod_{i=1}^{M_A} p(a=\mu_i|x=i,\lambda)}. \tag{2.44}$$

It readily follows that the new local model

$$p'(a,b|x,y) = \sum_{\mu} p'(\mu) p'(a|x,\mu) p'(b|y,\mu) \tag{2.45}$$

reproduces the original behaviour $p(a,b|x,y)$. In this new local model, only Alice's response function is deterministic, and the hidden variable μ takes on $m_A^{M_A}$ possible values (the number of deterministic strategies available to Alice). The fact that this can be done without loss of generality will be important in section 3.1.

2.3 THE CHSH INEQUALITY AND QUANTUM NON-LOCALITY

The simplest non trivial Bell scenario is the one with binary inputs and outputs, i.e. $M_A = M_B = m_A = m_B = 2$. For this case, utilizing a symmetric encoding of the outputs $a, b \in \{-1, 1\}$, all local behaviours satisfy the following inequality:

$$S = \langle a_0 b_0 \rangle + \langle a_0 b_1 \rangle + \langle a_1 b_0 \rangle - \langle a_1 b_1 \rangle \leq 2, \tag{2.46}$$

where $\langle a_x b_y \rangle = \sum_{a,b \in \{-1,1\}} abp(a, b|x, y)$. This is known as the CHSH inequality, after its discoverers, Clauser, Horne, Shimony and Holt (CLAUSER et al., 1969). This inequality (along with all its possible permutations of inputs and outputs) and the positivity constraints on the probabilities completely characterize the local polytope in the binary scenario (FINE, 1982). Naturally, it is also valid in scenarios with more inputs and outputs, but in general it is no longer the only non trivial facet inequality.

So far, it is by no means obvious that quantum behaviours (equation 2.16) are potentially incompatible with a local model description (equation 2.17), which is exactly the statement of Bell's theorem (BELL, 1964). However, the quantum scenario characterized by:

$$\rho = |\psi^-\rangle \langle \psi^-| , \tag{2.47}$$

$$\left\{\Pi_a^{x=0}\right\} = \mathrm{Proj}\left(\sigma_x\right), \tag{2.48}$$

$$\left\{\Pi_a^{x=1}\right\} = \mathrm{Proj}\left(\sigma_z\right), \tag{2.49}$$

$$\left\{\Pi_b^{y=0}\right\} = \mathrm{Proj}\left(\frac{-\sigma_x - \sigma_z}{\sqrt{2}}\right), \tag{2.50}$$

$$\left\{\Pi_b^{y=1}\right\} = \mathrm{Proj}\left(\frac{\sigma_z - \sigma_x}{\sqrt{2}}\right), \tag{2.51}$$

violates the CHSH inequality 2.46 with $S = 2\sqrt{2}$ (NIELSEN; CHUANG, 2000). In fact, $S = 2\sqrt{2}$ is the largest possible quantum violation of the CHSH inequality (CIREL'SON, 1980). In these equations, $|\psi^-\rangle = \frac{|01\rangle - |10\rangle}{\sqrt{2}}$ denotes the singlet state ($|0\rangle$ and $|1\rangle$ are eigenstates of σ_z), σ_x and σ_z are the usual Pauli operators, and $\mathrm{Proj}(L)$ denotes the set of projector operators in the eigensubspaces of L.

This proves that some quantum behaviours are incompatible with an explanation in terms of local hidden variable, a fact known as Bell's theorem.

2.4 NETWORK NON-LOCALITY

In (BRANCIARD; GISIN; PIRONIO, 2010), the authors took inspiration in entanglement swapping protocols and considered a scenario with 3 parties and 2 independent local hidden variables as shown in figure 4 below.

Figure 4 – Bilocal scenario. The outputs of each party a, b and c are represented by green circles, while the inputs x, y and z are represented by blue squares (also known as measurement settings). The local hidden variables λ and μ are represented by red triangles. In contrast to standard Bell scenarios, the multiple hidden variables are not distributed to all parties and are assumed to be statistically independent.

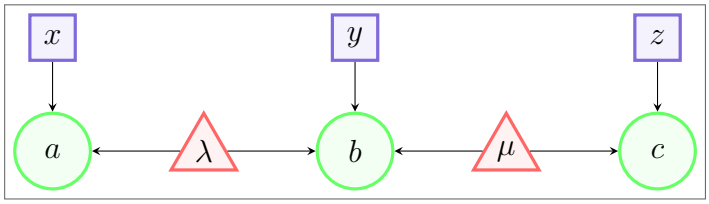

Source: personal archive

In this so called bilocal scenario, there is a feature that was not present in the standard Bell scenario we have been exploring so far, namely the presence of more than 1 hidden variable, along with the assumption of statistical independence between the hidden variables. This leads to a natural generalization from Bell scenarios to network scenarios. In a network scenario, there are multiple local hidden variables (or quantum states in the case of quantum networks) and not all parties have access to all hidden variables, which are assumed to be statistically independent. In order to define local and quantum behaviours in the case of networks, it is perhaps best to work with an example. Consider the network depicted in figure 5.

As was the case with standard Bell scenarios, we are interested in the probability distribution $p(\text{outputs}|\text{inputs})$, which is $p(a, b, c, d|x, y, z, w)$ for the network of figure 5. The behaviour is called network-local if there exists probability distributions $p(\lambda)$ and $p(\mu)$ and response functions $p(a|x, \lambda)$, $p(b|y, \lambda, \mu)$, $p(c|z, \lambda)$ and $p(d|w, \mu)$ such that

$$p(a, b, c, d|x, y, z, w) = \int d\lambda \, d\mu \, p(\lambda)p(\mu)p(a|x, \lambda)p(b|y, \lambda, \mu)p(c|z, \lambda)p(d|w, \mu). \quad (2.52)$$

Notice the independence of the hidden variables $p(\lambda, \mu) = p(\lambda)p(\mu)$. In the case of a quantum network, the local hidden variables λ and μ are substituted by quantum states ρ and σ, as shown in figure 6 below.

Figure 5 – Example of a generic local network. The outputs of each party a, b, c and d are represented by green circles, while the inputs x, y, z and w are represented by blue squares (also known as measurement settings). The local hidden variables λ and μ are represented by red triangles. A network local behaviour $p(a,b,c,d|x,y,z,w)$ in such a scenario can always be cast into the form of equation 2.52 (notice the statistical independence between λ and μ).

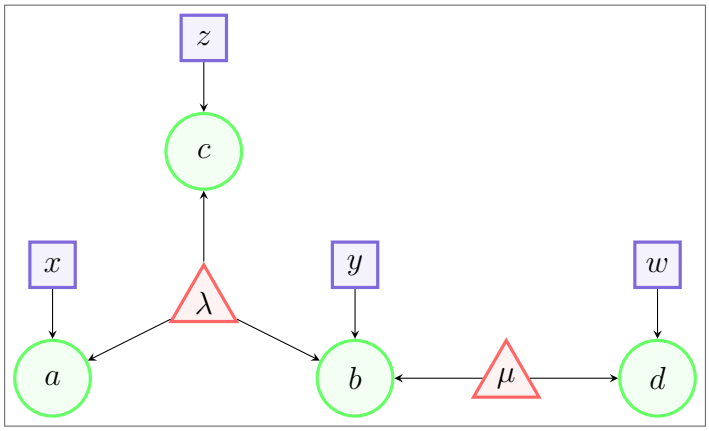

Source: personal archive

Figure 6 – Example of a generic quantum network. The outputs of each party a, b, c and d are represented by green circles, while the inputs x, y, z and w are represented by blue squares (also known as measurement settings). The quantum states ρ and σ are represented by the bare symbols in no geometric form. A network quantum behaviour $p(a,b,c,d|x,y,z,w)$ in such a scenario can always be cast into the form of equation 2.61 (notice that the global state is a product state $\rho \otimes \sigma$, which reflects the source independence condition).

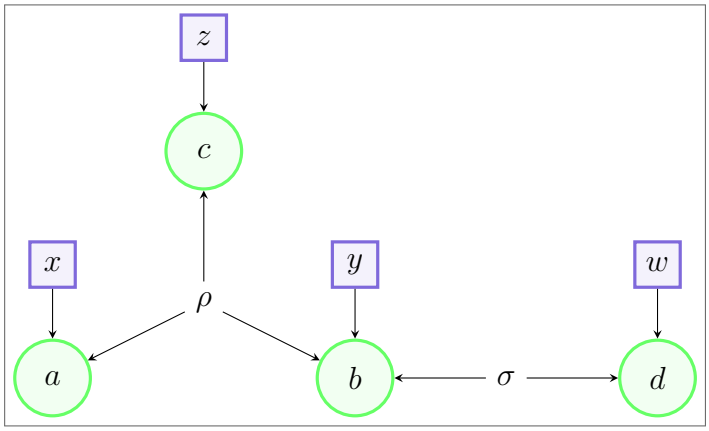

Source: personal archive

The behaviour $p(a,b,c,d|x,y,z,w)$ is said to be network-quantum if there exists quantum

states ρ and σ and POVMs $\{\Pi_a^x\}$, $\{\Pi_b^y\}$, $\{\Pi_c^z\}$ and $\{\Pi_d^w\}$ such that

$$\Pi_a^x \geq 0, \qquad \forall a, x, \tag{2.53}$$

$$\Pi_b^y \geq 0, \qquad \forall b, y, \tag{2.54}$$

$$\Pi_c^z \geq 0, \qquad \forall c, z, \tag{2.55}$$

$$\Pi_d^w \geq 0, \qquad \forall d, w, \tag{2.56}$$

$$\sum_a \Pi_a^x = I_A, \qquad \forall x, \tag{2.57}$$

$$\sum_b \Pi_b^y = I_B, \qquad \forall y, \tag{2.58}$$

$$\sum_c \Pi_c^z = I_C, \qquad \forall z, \tag{2.59}$$

$$\sum_d \Pi_d^w = I_D, \qquad \forall w, \tag{2.60}$$

$$p(a, b, c, d|x, y, z, w) = \mathrm{Tr}\left[(\rho \otimes \sigma)\left(\Pi_a^x \otimes \Pi_b^y \otimes \Pi_c^z \otimes \Pi_d^w\right)\right]. \tag{2.61}$$

In the case of a quantum network, the condition of statistical independence between local hidden variables turns into the requirement that the full quantum state can be written as a product state $\rho \otimes \sigma$, which implies that ρ and σ are independently prepared, thereby sharing neither classical nor quantum correlations.

The problem of fully characterizing the local set in network scenarios turns out to be a challenging one, mainly because the network local set is no longer convex. So much so that the study of network-local correlations has become an active area of research, with many open problems. One of the few general facts known to be true for network scenarios is that they are characterised by a finite number of polynomial inequalities (FRITZ, 2012) (ROSSET; GISIN; WOLFE, 2017). A good review of the progress made so far regarding network non-locality can be found in (TAVAKOLI et al., 2021).

In chapter 3, a numerical procedure for finding an explicit network-local model that reproduces a given behaviour will be presented. Then, this tool will be applied to solve interesting problems in two network scenarios: the bilocal one already shown in figure 4 and also the triangle scenario with no inputs. So it is important to review some important results obtained for these two network topologies.

2.5 THE TRIANGLE SCENARIO WITH NO INPUTS

The introduction of network scenarios leads to the possibility of quantum non-locality even in the case when the parties do not have a choice of measurement, i.e. when there are no inputs. This is not possible in standard Bell non-locality, where it is essential not only that the parties have a choice of at least 2 measurement settings, but also that this choice can be made independently of the system measured by the parties (sometimes referred to as the free will assumption). In network non-locality, the issue of free will can be entirely removed from the picture with the introduction of the more explicit assumption of source independence. The simplest case where non-locality without inputs can manifest is the triangle scenario shown in figure 7.

Figure 7 – Triangle scenario with no inputs. The outputs of each party a, b and c are represented by green circles. The local hidden variables α, β and γ are represented by red triangles. Notice the lack of input choice for the parties. This is the simplest scenario that exhibits non-locality without inputs.

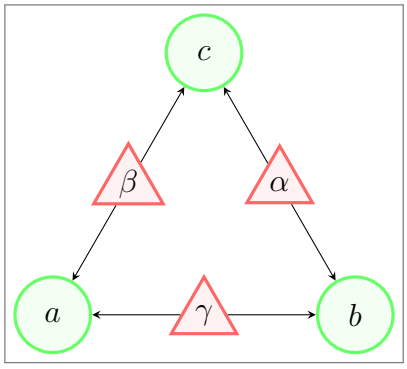

Source: personal archive

In (FRITZ, 2012) it is shown that every quantum correlation that violates the CHSH inequality in the standard Bell scenario can give rise to a behaviour $p(a, b, c)$ that is non-local in the triangular scenario of figure 7. Although this result proves the existence of quantum non-locality without inputs in networks, this non-locality stems directly from the standard bipartite Bell non-locality, which suggests that it is not a genuinely new kind of non-locality specific to network configurations. However, in (RENOU et al., 2019a), the authors obtain a non-local quantum correlation for the triangle scenario whose non-locality seems to be genuine to networks. So it might even possible that the standard Bell non-locality is actually a special case of the more fundamental phenomenon of non-locality without inputs in networks.

Now consider the problem of ascertaining if a given behaviour $p(a, b, c)$ is compatible with the network-local model of figure 7. A promising advancement made in the direction of

solving these kinds of problems (not only for the triangle scenario, but also for general network topologies) is the inflation technique (WOLFE; SPEKKENS; FRITZ, 2019). With this technique it is possible to derive Bell-like inequalities that are necessary conditions for network-locality (in general they are not sufficient though[4]). When applying inflation to the triangle scenario with binary outputs ($m_A = m_B = m_C = 2$) and symmetric encoding $a, b, c \in \{-1, 1\}$, one finds the following inequality:

$$\langle ac \rangle + \langle bc \rangle - \langle a \rangle \langle b \rangle \leq 1. \tag{2.62}$$

Although inequality 2.62 is not a sufficient condition for network-locality, its violation is enough to witness the non-locality of some interesting distributions. Consider for example the so called Greenberger-Horne-Zeilinger (GHZ) distribution, inspired by the well known GHZ quantum state (GREENBERGER et al., 1990):

$$p_{\mathsf{GHZ}}(a, b, c) = \begin{cases} 1/2, & \text{if } a = b = c \\ 0, & \text{otherwise} \end{cases}. \tag{2.63}$$

Since $a, b, c \in \{-1, 1\}$, this distribution satisfies $\langle ac \rangle = \langle bc \rangle = 1$ and $\langle a \rangle = \langle b \rangle = 0$, therefore it violates 2.62. Thus, it is not network-local. Incidentally, neither can it be generated by 3 independent sources distributing quantum states, since network-quantum behaviours also do not violate inequality 2.62 (WOLFE; SPEKKENS; FRITZ, 2019). Consider now the uniformly random distribution:

$$p_0(a, b, c) = \frac{1}{8}, \qquad \forall a, b, c. \tag{2.64}$$

This one is obviously local, since it can be realized by Alice, Bob and Charles randomly determining their outputs with equal probability. What about the mixed distribution $p = (1-v)p_0 + vp_{\mathsf{GHZ}}$? It is expected that for visibilities greater than some threshold v^* this mixed distribution ceases to be local. The problem of estimating v^* will be addressed in section 3.3

2.6 THE BILOCAL SCENARIO

The bilocal scenario (figure 4) was already introduced when discussing the concept of network-nonlocality. It was the first network scenario to be proposed (BRANCIARD; GISIN; PIRONIO, 2010). As we did for the triangle scenario, consider the problem of ascertaining if a

[4] I should add that the inflation technique can be used to provide asymptotically tight criteria for network-locality (NAVASCUÉS; WOLFE, 2020), albeit at the cost of exponentially increasing computational cost.

given behaviour $p(a,b,c|x,y,z)$ is compatible with the network-local model of figure 4. The bilocal scenario was thoroughly studied in (BRANCIARD et al., 2012), where a necessary condition for network-locality was proven. This condition is called the BRGP inequality, after its discoverers, Branciard, Gisin, Rosset and Pironio. In the case of binary inputs and outputs ($a,b,c,x,y,z \in \{0,1\}$), this inequality is expressed in terms of the quantities I and J, defined as:

$$I = \frac{1}{4} \sum_{x,z,a,b,c} (-1)^{a+b+c} p(a,b,c|x,y=0,z), \tag{2.65}$$

$$J = \frac{1}{4} \sum_{x,z,a,b,c} (-1)^{a+b+c+x+z} p(a,b,c|x,y=1,z), \tag{2.66}$$

and the BRGP inequality reads:

$$\sqrt{|I|} + \sqrt{|J|} \leq 1. \tag{2.67}$$

The BRGP inequality 2.67 is a necessary condition for network-locality, but in general it is not a sufficient one. However, it was shown to be tight in a particular 2-dimensional slice of the probability space. Consider the distributions p_I, p_J and p_0 defined as:

$$p_I(a,b,c|x,y,z) = \frac{1}{8}\left[1 + \delta_{y,0}(-1)^{a+b+c}\right], \tag{2.68}$$

$$p_J(a,b,c|x,y,z) = \frac{1}{8}\left[1 + \delta_{y,1}(-1)^{x+z+a+b+c}\right], \tag{2.69}$$

$$p_0(a,b,c|x,y,z) = \frac{1}{8}, \qquad \forall a,b,c,x,y,z, \tag{2.70}$$

and the behaviours $p(a,b,c|x,y,z)$ given by:

$$p = Ip_I + Jp_J + (1-I-J)p_0, \tag{2.71}$$

where the dependency on a, b, c, x, y and z has been omitted to keep the notation clean and $I, J \in [-1,1]$. The correlations 2.71 define a 2-dimensional slice of the probability space in which the BRGP inequality 2.67 is tight (BRANCIARD et al., 2012). But what about in other 2-dimensional sections? The problem of estimating the network-local boundary for slices where the BRGP inequality is not tight will be addressed in section 3.4

3 DETERMINATION OF LOCAL MODELS

Having introduced the concepts of Bell non-locality and network non-locality in chapter 2, we are almost ready to present the proposed numerical tool for finding explicit network local models and its applications to the problems introduced in sections 2.5 and 2.6. The last missing ingredient is a powerful result that provides an upper bound on the cardinality of hidden variables in network scenarios. This result is explained in section 3.1. The main idea behind the numerical tool is then shown in section 3.2. Finally, its application to the triangle and bilocal topologies is presented in sections 3.3 and 3.4, respectively.

3.1 BOUNDS ON HIDDEN VARIABLES CARDINALITY

In (ROSSET; GISIN; WOLFE, 2017) it was proven that the cardinalities of local hidden variables in networks can always be assumed to be finite. More than that, the following procedure provides an upper bound for the cardinality of a given hidden variable λ:

1. Identify the parties connected to λ. The outputs and inputs of these parties are collected in the vectors $\overline{a} = (a_1, a_2, \ldots)$ and $\overline{x} = (x_1, x_2, \ldots)$. The outputs and inputs of the remaining parties are collected in the vectors $\overline{b} = (b_1, b_2, \ldots)$ and $\overline{y} = (y_1, y_2, \ldots)$.

2. Using equation 2.29, calculate the no-signalling dimensions of the behaviours $p\left(\overline{a}, \overline{b}|\overline{x}, \overline{y}\right)$ and $p\left(\overline{b}|\overline{y}\right)$, denoted by $D_{\mathcal{NS}}(\mathcal{P}_{AB})$ and $D_{\mathcal{NS}}(\mathcal{P}_B)$.

3. The cardinality of λ, denoted by c_λ, is bounded without loss of generality by the following expression:

$$c_\lambda \leq D_{\mathcal{NS}}(\mathcal{P}_{AB}) - D_{\mathcal{NS}}(\mathcal{P}_B). \tag{3.1}$$

As an example, consider the triangle network with binary outputs and no inputs (figure 7). The hidden variable α is distributed to parties B and C, while A does not receive information from α. Hence, in the notation of (ROSSET; GISIN; WOLFE, 2017), $p\left(\overline{a}, \overline{b}|\overline{x}, \overline{y}\right) = p(a, b, c)$ and $p\left(\overline{b}|\overline{y}\right) = p(a)$. The no-signalling dimensions of these behaviour spaces are $D_{\mathcal{NS}}(\mathcal{P}_{AB}) = 7$ and $D_{\mathcal{NS}}(\mathcal{P}_B) = 1$, and the application of equation 3.1 implies that the cardinality c_α can be taken to be less than or equal to 6. By symmetry, the same can be said of the cardinalities c_β and c_γ.

In some cases this bound can be improved by enumerating the deterministic strategies of one of the parties. Consider for example the bilocal network (figure 4) with binary inputs and outputs for all parties. The parties connected to λ are A and B, so the appropriate distributions for calculating c_λ are $p\left(\overline{a},\overline{b}|\overline{x},\overline{y}\right) = p(a,b,c|x,y,z)$ and $p\left(\overline{b}|\overline{y}\right) = p(c|z)$. By using equation 2.29, the dimensions of these behaviour spaces are $D_{\mathcal{NS}}(\mathcal{P}_{AB}) = [2(2-1)+1]^3 - 1 = 26$ and $D_{\mathcal{NS}}(\mathcal{P}_B) = [2(2-1)+1] - 1 = 2$. Hence, using equation 3.1, the cardinality of λ is bounded by $26 - 2 = 24$. The same upper bound applies also to the cardinality of μ, by symmetry. However, there are only 4 possible deterministic strategies for Alice, as well as for Charles. Therefore, the upper bounds on the cardinalities can be reduced even further to $c_\lambda, c_\mu \leq 4$ (see the discussion at the end of section 2.2).

3.2 REPRESENTATION OF LOCAL MODELS

A local model with discrete hidden variables with known cardinality can be represented by 1-dimensional arrays $p_\lambda, p_\mu, \ldots$ representing the probability distributions of the hidden variables and multidimensional arrays $p_A, p_B, \ldots$ representing the response functions of each party. A specific hidden variable array p_λ must have $c_\lambda - 1$ elements representing the probabilities that λ assumes different values:

$$p_\lambda[i] = p(\lambda = i), \tag{3.2}$$

with $i \in \{1, 2, \ldots, c_\lambda - 1\}$. Only $c_\lambda - 1$ probabilities need to be specified because of the normalization condition $\sum_{i=1}^{c_\lambda} p(\lambda = i) = 1$.

Now consider one party A that receives hidden variables $\lambda_1, \ldots, \lambda_n$. The response function $p(a|x, \lambda_1, \ldots, \lambda_n)$ can then be represented by a multidimensional array p_A such that:

$$p_A[i, j, k, \ldots, l] = p(a = i|x = j, \lambda_1 = k, \ldots, \lambda_n = l), \tag{3.3}$$

with $i \in \{1, 2, \ldots, m_A - 1\}$, $j \in \{1, 2, \ldots, M_A\}$, $k \in \{1, 2, \ldots, c_{\lambda_1}\}$, …, $l \in \{1, 2, \ldots, c_{\lambda_n}\}$. The indexing convention for the response function arrays is always the following: the first index is the output value; the second input is the input value; and all the other indexes are the values of the hidden variables available to that party. Notice that the output index i only needs to run from 1 to $m_A - 1$ because of the normalization condition $\sum_{i=1}^{m_A} p(a = i|x, \lambda_1, \ldots, \lambda_n) = 1$.

Given the hidden variables arrays $p_\lambda, p_\mu, \ldots$ and the parties arrays $p_A, p_B, \ldots$, all the pro-

babilities $p(a, b, \ldots|x, y, \ldots)$ can be calculated:

$$p(a, b, \ldots|x, y, \ldots) = \sum_{i,j,\ldots} \{p_\lambda[i]p_\mu[j]\ldots p_A[a, x, \ldots]p_B[b, y, \ldots]\ldots\}\,. \tag{3.4}$$

Therefore, the problem of finding a local model for a given behaviour $p^*(a, b, \ldots|x, y, \ldots)$ can be reduced to a constrained optimization problem on the elements of $p_\lambda, p_\mu, \ldots$ and $p_A, p_B, \ldots$:

$$\begin{aligned}
&\min_{p_\lambda, p_\mu, \ldots, p_A, p_B, \ldots} \sum_{a,b,\ldots,x,y,\ldots} [p(a, b, \ldots|x, y, \ldots) - p^*(a, b, \ldots|x, y, \ldots)]^2 \\
&\text{s.t.} \quad p_\lambda, p_\mu, \ldots, p_A, p_B, \ldots \geq 0 \\
&\qquad \sum_i p_\lambda[i] \leq 1 \\
&\qquad \sum_i p_\mu[i] \leq 1 \\
&\qquad \ldots \\
&\qquad \sum_i p_A[i, \ldots] \leq 1 \\
&\qquad \sum_i p_B[i, \ldots] \leq 1 \\
&\qquad \ldots \\
&\text{where } p(a, b, \ldots|x, y, \ldots) = \sum_{i,j,\ldots} \{p_\lambda[i]p_\mu[j]\ldots p_A[a, x, \ldots]p_B[b, y, \ldots]\ldots\}
\end{aligned} \tag{3.5}$$

In order to apply this idea to solve interesting problems regarding the bilocal and triangle topologies (figures 4 and 7), two Python modules named bilocal.py and triangle.py were created. The code and documentation are available at github.com/mariofilho281/localmodels. In these two modules, the optimization problem 3.5 is solved with a trust-region algorithm for constrained optimization available at the SciPy package (VIRTANEN et al., 2020). This algorithm deals with inequality constraints by employing the barrier method, which reduces the original problem to a sequence of equality constrained problems. Each of these subproblems is then solved using a trust-region sequential quadratic programming (SQP) with the projected conjugate gradient (CG) method (BYRD; HRIBAR; NOCEDAL, 1999).

Finally, one important remark is that in standard Bell non-locality, the problem of finding a local model for a given behaviour (if one such model exists) is substantially easier. In fact, it reduces to a feasibility problem in linear programming, for which there are algorithms that can provide an explicit model in case the behaviour is local, or a Bell inequality violated by the behaviour in case it is not local (SCARANI, 2019). In network non-locality, such methods are

not applicable because the problem of finding a network local model is no longer an instance of convex optimization.

3.3 TRIANGLE NETWORK

As a first application, let us consider the following question: for which visibilities can the GHZ distribution (equation 2.63) be obtained as a trilocal model in the triangle scenario?

When solving problem 3.5 for a GHZ distribution in triangle network with varying visibilities, the optimization error as a function of the visibility can be seen in figure 8. In order to have a meaningful quantity to report, the optimization error of problem 3.5 if first divided by 8 (the number of entries in the probability distribution $p(a, b, c)$) and then taken the square root, before being plotted. The y-axis of figure 8 can therefore be interpreted as a mean error in the probabilities, when comparing the target distribution and the numerical solution. Notice that for visibilities greater than $v^* \approx 1/3$, the numerical optimization can no longer find a local model for the desired behaviour, a strong indication that the distribution ceases to be network-local for $v > 1/3$.

Numerical procedures such as the one developed here do not serve as a mathematical proof of non-locality, although they certainly provide evidence in this direction. They can however be used for proving the locality of a given behaviour. Let us consider the GHZ distribution with $v = 1/3$.

When solving optimization problem 3.5 for $v = 0.33$, one possible model[1] has the following

[1] The solution of problem 3.5 is not unique. Since the initial guess is randomized, each instance the numerical routine is performed, slightly different results might ensue. Also, sometimes the optimization algorithm sometimes fails to converge to an acceptable solution, specially when near the non-locality threshold. In such cases, it might take a few trials to get a model to a local distribution.

Figure 8 – Optimization error as a function of the visibility of the GHZ distribution. For visibilities $v \leq 1/3$, the error reaches values very close to zero, indicating that these behaviours are network local. For visibilities $v > 1/3$, the solver can no longer achieve low optimization errors, indicating that these behaviours are most likely not network local.

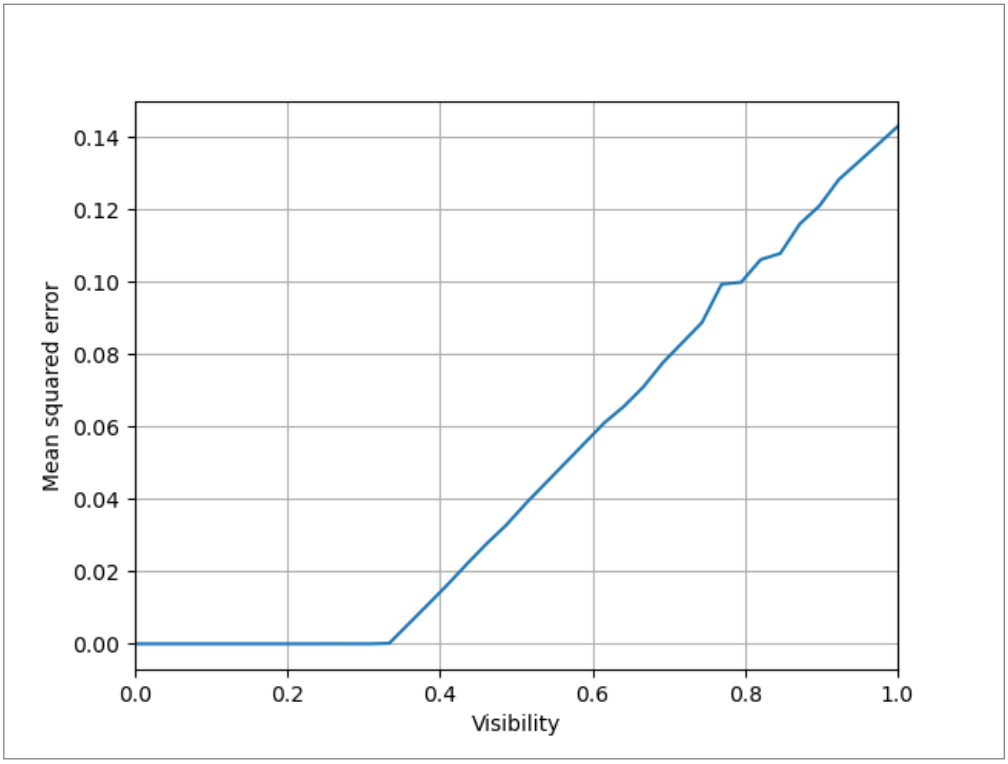

Source: personal archive

distributions in the hidden variables:

$$p_\alpha = \begin{pmatrix} 5.515\,129 \times 10^{-4} \\ 4.988\,952 \times 10^{-1} \\ 4.462\,493 \times 10^{-4} \\ 4.775\,986 \times 10^{-4} \\ 4.685\,608 \times 10^{-4} \\ 4.991\,608 \times 10^{-1} \end{pmatrix}, \quad p_\beta = \begin{pmatrix} 4.680\,312 \times 10^{-4} \\ 4.798\,686 \times 10^{-4} \\ 4.717\,101 \times 10^{-4} \\ 4.768\,658 \times 10^{-4} \\ 4.988\,352 \times 10^{-1} \\ 4.989\,683 \times 10^{-1} \end{pmatrix}, \quad p_\gamma = \begin{pmatrix} 4.717\,443 \times 10^{-4} \\ 4.626\,071 \times 10^{-4} \\ 1.678\,008 \times 10^{-1} \\ 5.408\,369 \times 10^{-4} \\ 1.675\,872 \times 10^{-1} \\ 6.631\,367 \times 10^{-1} \end{pmatrix}. \tag{3.6}$$

For this initial discussion, the response functions are not important. I also would like to add that in order to better communicate the local model obtained, the arrays of equation 3.6 have been appended with the last probability that can be determined from the normalization condition. So contrary to the generic array p_λ of equation 3.2, the objects of equation 3.6 do sum up to unity. A striking feature of p_α, p_β and p_γ in equations 3.6 is that some probabilities seem to be extremely low: α is predominantly restricted to the 2nd and 6th values, β to the

5th and 6th, and finally γ to the 3rd, 5th and 6th. A natural question then arises: can the same behaviour with $v = 0.33$ be obtained with reduced cardinalities $c_\alpha = 2$, $c_\beta = 2$ and $c_\gamma = 3$? Running the optimization again for $v = 0.33$ with these reduced cardinalities usually takes more attempts to produce an acceptable model (a consequence of the fact that now the solver has less degrees of freedom to work with), but eventually lead to solutions such as the one below:

$$p_\alpha = \begin{pmatrix} 0.49947714 \\ 0.50052286 \end{pmatrix}, \qquad p_\beta = \begin{pmatrix} 0.49982998 \\ 0.50017002 \end{pmatrix}, \qquad p_\gamma = \begin{pmatrix} 0.16934519 \\ 0.16875225 \\ 0.66190257 \end{pmatrix}, \tag{3.7}$$

$$p_A = \begin{pmatrix} 0.01142633 & 0.9971927 & 0.99765428 \\ 0.00331543 & 0.99337977 & 0.00221306 \end{pmatrix}, \tag{3.8}$$

$$p_B = \begin{pmatrix} 0.00306624 & 0.00958604 \\ 0.99031315 & 0.99664584 \\ 0.00226471 & 0.99767491 \end{pmatrix}, \tag{3.9}$$

$$p_C = \begin{pmatrix} 0.49971671 & 0.00113535 \\ 0.99882767 & 0.49961629 \end{pmatrix}. \tag{3.10}$$

In the triangle scenario with no inputs and binary outputs, the response functions are simple enough to be represented by the 2-dimensional arrays of equations 3.8, 3.9 and 3.10. Encoding the outputs as $a, b, c \in \{0, 1\}$, they represent the probability that each party outputs 0 for different values of their respective hidden variables. Explicitly:

$$p(a = 0|\beta = i, \gamma = j) = p_A[i, j], \tag{3.11}$$

$$p(b = 0|\gamma = i, \alpha = j) = p_B[i, j], \tag{3.12}$$

$$p(c = 0|\alpha = i, \beta = j) = p_C[i, j], \tag{3.13}$$

where i indexes the rows and j indexes the columns (just like matrices). Obviously, the probability that the parties output 1 can be readily obtained by normalization.

The arrays in equations 3.7, 3.8, 3.9 and 3.10 look like numerical estimates of the following

arrays:

$$p_\alpha = \begin{pmatrix} 1/2 \\ 1/2 \end{pmatrix}, \qquad p_\beta = \begin{pmatrix} 1/2 \\ 1/2 \end{pmatrix}, \qquad p_\gamma = \begin{pmatrix} 1/6 \\ 1/6 \\ 2/3 \end{pmatrix}, \tag{3.14}$$

$$p_A = \begin{pmatrix} 0 & 1 & 1 \\ 0 & 1 & 0 \end{pmatrix}, \tag{3.15}$$

$$p_B = \begin{pmatrix} 0 & 0 \\ 1 & 1 \\ 0 & 1 \end{pmatrix}, \tag{3.16}$$

$$p_C = \begin{pmatrix} 1/2 & 0 \\ 1 & 1/2 \end{pmatrix}. \tag{3.17}$$

This new proposed model has deterministic response functions for Alice and Bob. In order to express them more compactly one can always permute the labels of γ so that the arrays change to:

$$p_\alpha = \begin{pmatrix} 1/2 \\ 1/2 \end{pmatrix}, \qquad p_\beta = \begin{pmatrix} 1/2 \\ 1/2 \end{pmatrix}, \qquad p_\gamma = \begin{pmatrix} 1/6 \\ 2/3 \\ 1/6 \end{pmatrix}, \tag{3.18}$$

$$p_A = \begin{pmatrix} 1 & 1 & 0 \\ 1 & 0 & 0 \end{pmatrix}, \tag{3.19}$$

$$p_B = \begin{pmatrix} 1 & 1 \\ 0 & 1 \\ 0 & 0 \end{pmatrix}, \tag{3.20}$$

$$p_C = \begin{pmatrix} 1/2 & 0 \\ 1 & 1/2 \end{pmatrix}. \tag{3.21}$$

This model reproduces the same behaviour as before. We permuted the labels of γ only so that we could represent the model in a more compact form. Encoding the hidden variables

as $\alpha \in \{0,1\}$, $\beta \in \{0,1\}$ and $\gamma \in \{0,1,2\}$ we have:

$$\alpha = \frac{1}{2}[0] + \frac{1}{2}[1], \tag{3.22}$$

$$\beta = \frac{1}{2}[0] + \frac{1}{2}[1], \tag{3.23}$$

$$\gamma = \frac{1}{6}[0] + \frac{2}{3}[1] + \frac{1}{6}[2], \tag{3.24}$$

$$a(\beta,\gamma) = \begin{cases} 0, & \text{if } \beta+\gamma \leq 1 \\ 1, & \text{otherwise} \end{cases}, \tag{3.25}$$

$$b(\gamma,\alpha) = \begin{cases} 0, & \text{if } \gamma \leq \alpha \\ 1, & \text{otherwise} \end{cases}, \tag{3.26}$$

$$c(\alpha,\beta) = \begin{cases} \frac{1}{2}[0] + \frac{1}{2}[1], & \text{if } \alpha = \beta \\ \beta, & \text{otherwise} \end{cases}, \tag{3.27}$$

where the notation $p_0[0] + p_1[1] + \cdots$ represents a random variable that assumes value 0 with probability p_0, 1 with probability p_1, and so on.

It turns out that this model reproduces exactly the GHZ distribution with visibility $v = 1/3$:

$$p(a,b,c) = \begin{cases} 1/4, & \text{if } a = b = c \\ 1/12, & \text{otherwise} \end{cases}. \tag{3.28}$$

I hope this section has successfully illustrated how the optimization problem 3.5 can be used to explicitly construct local models for a given behaviour. Before moving on to the next application, let us pursue one final investigation regarding the family of behaviours $p = (1-v)p_0 + vp_{\text{GHZ}}$. We have proven that p is network-local for $v = 1/3$. For $v = 0$, p is an uniformly random distribution, therefore it is network-local also in this case. Are we then allowed to draw the conclusion that p is network-local for all $v \in [0,1/3]$? At this point no, because the local set for the triangle scenario is not convex. In fact, as proven in (RENOU et al., 2019b), it is not even star-convex with respect to the uniform distribution p_0[2]. However, figure 8 certainly suggests that p is network-local for all $v \in [0,1/3]$. Indeed this is the case, because a local model for these visibilities can be constructed by augmenting the cardinality c_γ to 4 (so that $\gamma \in \{0,1,2,3\}$) and instructing Alice and Bob to uniformly randomize their outputs if they receive $\gamma = 3$. The following model reproduces the behaviour $p = (1-v)p_0 + vp_{\text{GHZ}}$

[2] A set $\mathcal{S}$ is star-convex with respect to the point p_0 if, and only if for every point $p \in \mathcal{S}$, all the points in the line segment joining p_0 and p also belong to $\mathcal{S}$.

for $v \in [0, 3]$:

$$\alpha = \frac{1}{2}[0] + \frac{1}{2}[1], \tag{3.29}$$

$$\beta = \frac{1}{2}[0] + \frac{1}{2}[1], \tag{3.30}$$

$$\gamma = \frac{v}{2}[0] + 2v[1] + \frac{v}{2}[2] + (1 - 3v)[3], \tag{3.31}$$

$$a(\beta, \gamma) = \begin{cases} \frac{1}{2}[0] + \frac{1}{2}[1], & \text{if } \gamma = 3 \\ 0, & \text{if } \beta + \gamma \leq 1 \\ 1, & \text{otherwise} \end{cases}, \tag{3.32}$$

$$b(\gamma, \alpha) = \begin{cases} \frac{1}{2}[0] + \frac{1}{2}[1], & \text{if } \gamma = 3 \\ 0, & \text{if } \gamma \leq \alpha \\ 1, & \text{otherwise} \end{cases}, \tag{3.33}$$

$$c(\alpha, \beta) = \begin{cases} \frac{1}{2}[0] + \frac{1}{2}[1], & \text{if } \alpha = \beta \\ \beta, & \text{otherwise} \end{cases}. \tag{3.34}$$

3.4 BILOCAL NETWORK

As a second application for the technique, let us consider the problem of finding an approximation for the boundary of the bilocal set in affine subspaces of dimension 2 in the no-signalling space[3]. The first affine subspace to be considered is one for which the local boundary is known to be the BRGP inequality (equation 2.67). Given the distributions p_I, p_J and p_0 of equations 2.68, 2.69 and 2.70, each ordered pair $(I, J) \in [-1, 1] \times [-1, 1]$ define a behaviour p according to equation 2.71. The coefficients I and J match the parameters that enter the BRGP expression (equations 2.65 and 2.66) (BRANCIARD et al., 2012).

Solving problem 3.5 for a rectangular grid of pairs (I, J), the optimization error can be seen in figure 9. Analogous to what was done in section 3.3, the optimization error of problem 3.5 is first divided by 64 (the number of entries in the probability distribution $p(a, b, c|x, y, z)$) and then taken the square root, before being plotted. The solid red line is the boundary of the

[3] Affine subspaces are generalizations of points, lines, planes and so forth to multiple dimensions. Consider for example a collection of n linearly independent points $P_1, \ldots, P_n$ in the euclidean space $\mathbb{R}^d$ The set of points P that be written as

$$P = \sum_k c_k P_k,$$

with $\sum_k c_k = 1$ constitutes an $(n-1)$-dimensional affine subspace of $\mathbb{R}^d$.

network-local set in this 2-dimensional slice given by the BRGP inequality 2.67. The first thing we notice is that the points inside this region exhibit optimization error close to 0, showing that the solver has found acceptable local models for them, which is expected. Also, behaviours outside the network-local boundary exhibit higher error, showing that the solver did not find faithful local models for them, which is also expected.

Figure 9 – Optimization error in the affine subspace spanned by the distributions 2.68-2.70. The solid red line is the bilocal boundary given by the BRGP inequality 2.67. For behaviours inside the boundary, the solver can get the optimization error close to zero. As we move away from the boundary to behaviours that are not bilocal, the error grows, as expected.

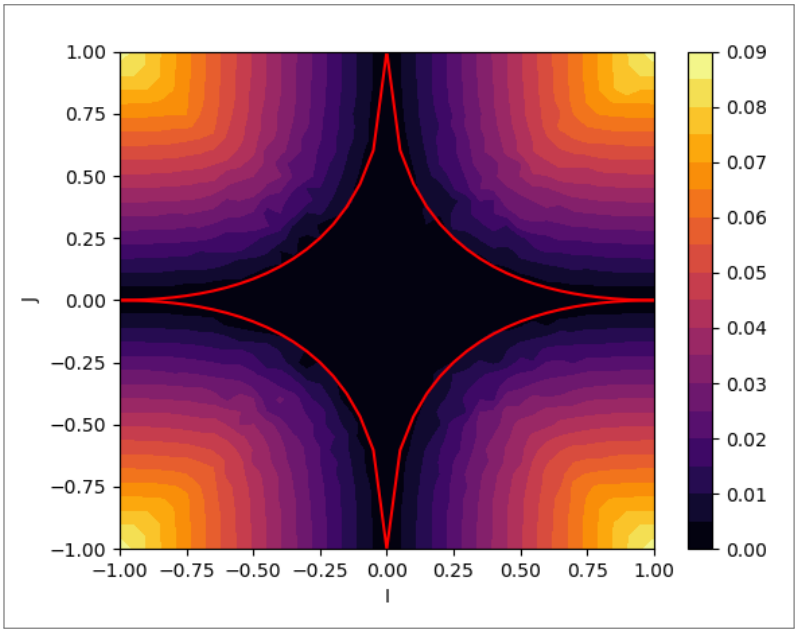

Source: personal archive

In order to extract an actual boundary between the local and non-local regions from the numerical procedure, a threshold for what is an acceptable optimization error must be established. This task can be done in the affine subspace spanned by the correlations p_I, p_J and p_0, since the exact boundary of the local region is known to be given by the BRGP inequality in this 2-dimensional slice. Analysing the dataset shown in figure 9, the region with a mean squared error in the probabilities less than 3.3×10^{-3} yields the highest agreement with the actual boundary. This region is displayed in figure 10a, for a rather coarse grid (this result will be refined in what follows).

Notice however that this threshold error leads to both false positives and false negatives, i.e. there are points with error less than 3.3×10^{-3} which are not bilocal and there are points with error greater than 3.3×10^{-3} which are bilocal. The error thresholds for regions without false positives and false negatives seem to be around 8.3×10^{-3} and 1.0×10^{-3} respectively. In

Figure 10 – Region of mean probability error less than a threshold E in the affine subspace spanned by the distributions 2.68-2.70. Results for a grid density of 420 points per unit area and 5 optimization trials per behaviour. (a) For $E = 3.3 \times 10^{-3}$, the closest agreement with the BRGP boundary is obtained. (b) For $E = 8.3 \times 10^{-3}$, all points outside the region are guaranteed not to be bilocal. (c) For $E = 1.0 \times 10^{-3}$, all points inside the region are guaranteed to be bilocal.

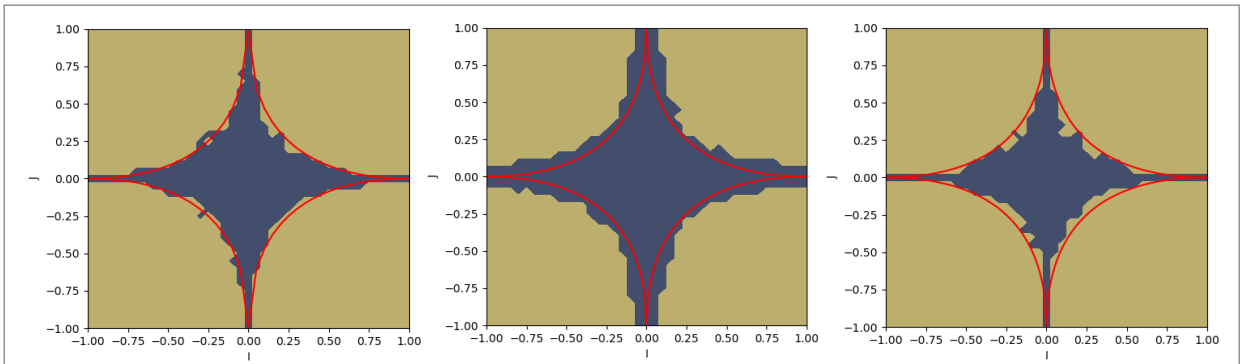

(a) $E = 3.3 \times 10^{-3}$ (b) $E = 8.3 \times 10^{-3}$ (c) $E = 1.0 \times 10^{-3}$

Source: personal archive

other words, the region with mean squared error less than 8.3×10^{-3} contains the bilocal set (see figure 10b), whereas the region with mean squared error less than 1.0×10^{-3} is contained in the bilocal set (see figure 10c).

These findings can be summarized in table 1. I should remark though that these thresholds are not absolute and should rather be taken merely as general guidelines when utilising the particular implementations of problem 3.5 provided in the modules bilocal.py and triangle.py. These values are expected to be different if we change the affine subspace under investigation, the density of points in the probability space, or the number of optimization trials for each behaviour. The thresholds of table 1 were obtained for the affine subspace spanned by the distributions of equations 2.68-2.70, a grid of 41×41 points in the probability space (density of 420 points per unit area), and 5 optimization trials for each behaviour.

Table 1 – Thresholds for the mean probability error in the probabilities

Error thresholds	Relation to the actual bilocal boundary
$E < 1.0 \times 10^{-3}$	The bilocal boundary is outside this region.
$E < 3.3 \times 10^{-3}$	Best approximation for the bilocal set.
$E < 8.3 \times 10^{-3}$	The bilocal boundary is inside this region.

Source: personal archive

If more precision is needed in the boundary estimation, the density of behaviours subjected to the optimization procedure can be increased only in regions with probability error sufficiently close to 3.3×10^{-3}, in order to keep the execution time manageable. The result of one such

procedure can be seen in figure 11, where the point density was increased to 10,100 points per unit area, much greater than the density of 420 points per unit area utilized in figure 10a.

Figure 11 – Numerical estimation of the bilocal boundary in the affine subspace spanned by the distributions 2.68-2.70. The error threshold is 3.3×10^{-3}, the same of figure 10a, but the point density was increased from 420 to 10,100 points per unit area, allowing for better resolution in the boundary estimation.

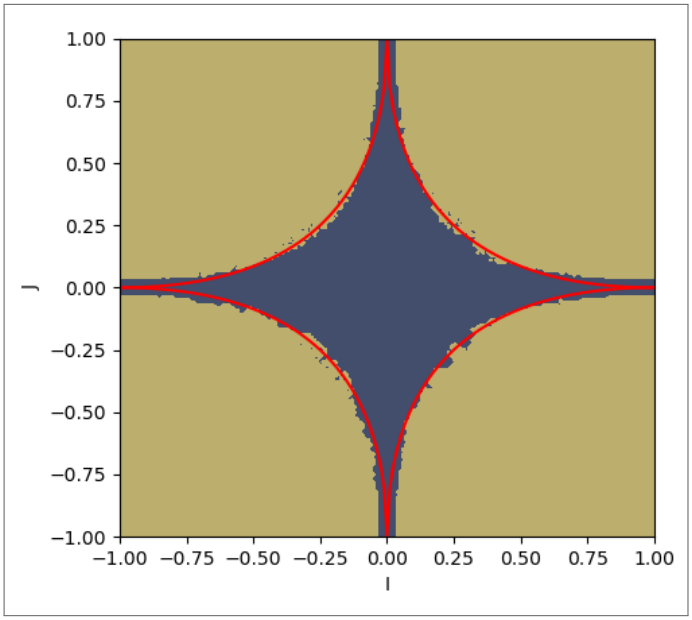

Source: personal archive

Now, let us move on to a 2-dimensional slice with no known tight inequality. Consider the following behaviours:

$$p_X(a,b,c|x,y,z) = \frac{1}{8}\left(\frac{1}{2} + \delta_{a,0}\right)\left[1 + \delta_{y,0}(-1)^{a+b+c}\right], \tag{3.35}$$

$$p_Y(a,b,c|x,y,z) = \frac{1}{8}\left(\frac{1}{2} + \delta_{a,0}\right)\left[1 + \delta_{y,1}(-1)^{z+a+b+c}\right], \tag{3.36}$$

$$p_0(a,b,c|x,y,z) = \frac{1}{8}\left(\frac{1}{2} + \delta_{a,0}\right). \tag{3.37}$$

For the remainder of this section, we will concern ourselves with the affine subspace spanned by the distributions 3.35-3.37, i.e. the set of behaviours $p(a,b,c|x,y,z)$ given by

$$p = Xp_X + Yp_Y + (1 - X - Y)p_0, \tag{3.38}$$

where the dependency on a, b, c, x, y and z has been omitted to keep the notation clean. Applying equations 2.65 and 2.66 to the distributions 3.35-3.37, the quantities I and J for

each of them are:

$$I_X = 1, \tag{3.39}$$

$$J_X = 0, \tag{3.40}$$

$$I_Y = 0, \tag{3.41}$$

$$J_Y = 0, \tag{3.42}$$

$$I_0 = 0, \tag{3.43}$$

$$J_0 = 0. \tag{3.44}$$

The parameters I and J are linear combinations of the probabilities $p(a, b, c|x, y, z)$. Therefore, it follows from equation 3.38 that

$$I_p = XI_X + YI_Y + (1 - X - Y)I_0 = X, \tag{3.45}$$

$$J_p = XJ_X + YJ_Y + (1 - X - Y)J_0 = 0. \tag{3.46}$$

Therefore, the only restriction enforced by the BRGP inequality $\sqrt{|I|} + \sqrt{|J|} \leq 1$ in this affine subspace is

$$|X| \leq 1. \tag{3.47}$$

Once again, we will work in the domain $(X, Y) \in [-1, 1] \times [-1, 1]$, but in this case, all the points of the square satisfy the BRGP inequality, which leaves the whole square region as potentially bilocal. Let us see if all these behaviours are really bilocal. The numerical procedure outlined above was performed for this affine subspace, with problem 3.5 being solved 5 times for each behaviour, initially with a density of 420 points per unit area and then refined to a density of 10.100 points per unit area. The optimization error of this procedure can be seen in figure 12 (the red dashed line will be explained shortly).

We see in figure 12 that the solver found acceptable bilocal models only for points in the darker regions of the square domain, revealing the non tightness of the BRGP inequality in this affine subspace. A numerical estimate of the actual bilocal boundary can be seen in figure 13 depicting the points with mean probability error less than 3.3×10^{-3}. Since this error threshold was obtained in another affine subspace, there is no guarantee that it functions properly on the subspace spanned by distributions 3.35-3.37. In fact, we shall next prove that all behaviours inside the square bounded the red dashed lines of figures 12 and 13 are bilocal.

The square bounded by the red dashed lines in figures 12 and 13 is characterized by the following inequality:

$$|X| + |Y| \leq 1. \tag{3.48}$$

Figure 12 – Optimization error in the affine subspace spanned by the distributions 3.35-3.37. The red dashed line is the conjectured boundary for the bilocal set in this 2-dimensional slice of the behaviour space. For behaviours inside the proposed boundary, the solver can get the optimization error close to zero. As we move away from this region, the error grows, indicating that the behaviours are no longer bilocal.

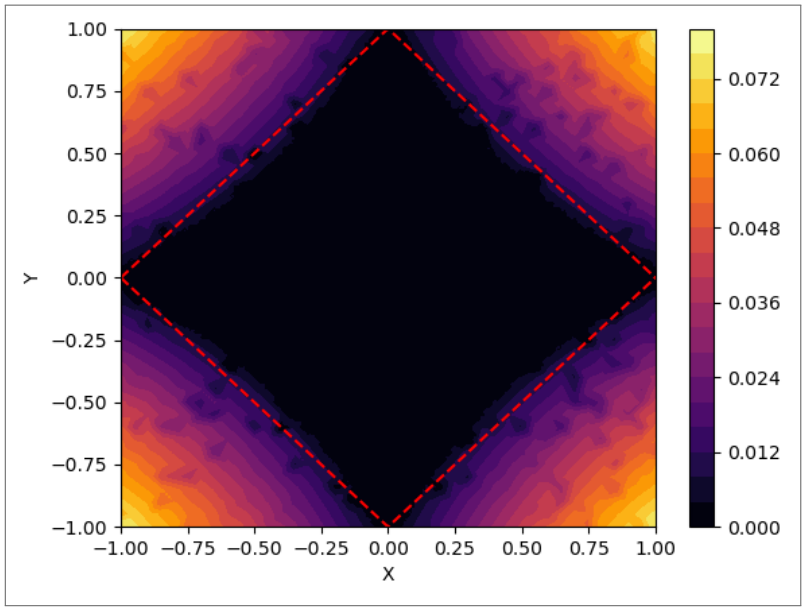

Source: personal archive

Figure 13 – Numerical estimation of the bilocal boundary in the affine subspace spanned by the distributions 3.35-3.37. The red dashed line is the conjectured boundary for the bilocal set in this 2-dimensional slice of the behaviour space. The error threshold is 3.3×10^{-3}, the same of figures 10a and 11. Since this threshold was obtained for another affine subspace (the one spanned by distributions 2.68-2.70), there is no guarantee it will yield the best agreement with the actual projection of the bilocal set in this affine subspace.

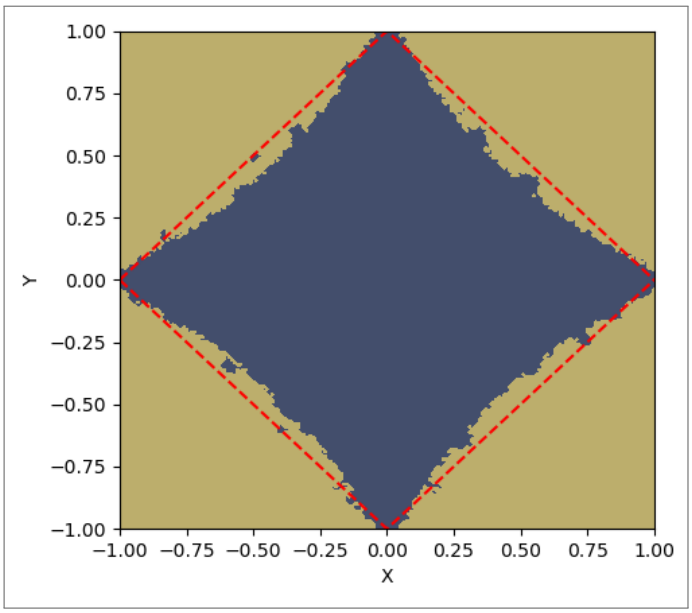

Source: personal archive

Focusing on the boundary behaviours located in the first quadrant, their probability distribution is given by

$$p(a,b,c|x,y,z) = \frac{1}{8}\left(\frac{1}{2} + \delta_{a,0}\right)\left[1 + X\delta_{y,0}(-1)^{a+b+c} + Y\delta_{y,1}(-1)^{z+a+b+c}\right], \tag{3.49}$$

with $X + Y = 1$.

Applying the same methods used in the end of section 3.3, it is possible to show that the following model reproduces these behaviours:

$$\lambda = \frac{3}{4}[0] + \frac{1}{4}[1], \tag{3.50}$$

$$\mu = \frac{Y}{2}[0] + \frac{X}{2}[1] + \frac{Y}{2}[2] + \frac{X}{2}[3], \tag{3.51}$$

$$a(x,\lambda) = \lambda, \tag{3.52}$$

$$b(y,\lambda,\mu) = \begin{cases} \frac{1}{2}[0] + \frac{1}{2}[1], & \text{if } \mu - y = 0, 2 \\ \lambda, & \text{if } \mu + y = 1 \\ 1 - \lambda, & \text{if } \mu + y = 3 \end{cases}, \tag{3.53}$$

$$c(z,\mu) = \begin{cases} 0, & \text{if } \mu - z = 0, 1 \\ 1, & \text{otherwise} \end{cases}. \tag{3.54}$$

Behaviours on the other 3 sides of the square ($X-Y = 1$, $X+Y = -1$ and $X-Y = -1$) can be reproduced by the same model if we perform the following operations:

i) exchange the output labels of Charles for the behaviours on the line $X - Y = 1$

ii) exchange the input labels of Charles for the behaviours on the line $X + Y = -1$

iii) exchange both the output and input labels of Charles for the behaviours on the line $X - Y = -1$

It has therefore been proved that all behaviours on the red dashed lines of figures 12 and 13 are bilocal. Finally, the behaviour at the square center $X = Y = 0$ is characterized by a factorized probability distribution

$$p_0(a,b,c|x,y,z) = \left(\frac{1}{4} + \frac{1}{2}\delta_{a,0}\right)\left(\frac{1}{2}\right)\left(\frac{1}{2}\right) = p(a|x)p(b|y)p(c|z). \tag{3.55}$$

Thus, the projection of the bilocal set onto this affine subspace is star-convex with respect to the center behaviour p_0, as proven in (BRANCIARD et al., 2012). Therefore, it follows that all behaviours that satisfy inequality 3.48 are bilocal.

In order to get stronger numerical evidence that inequality 3.48 is indeed the boundary of the bilocal set in this affine subspace, the optimization problem 3.5 was solved for 21 points in each of 3 lines characterized by

$$X + Y = 1 + \epsilon, \tag{3.56}$$

with $\epsilon \in \{-0.01, 0, 0.01\}$. The numerical procedure was run 30 times per behaviour, much greater than the 5 trials per behaviour used to generate figures 12 and 13. The results of this can be seen in figure 14. The first and last green points, as well as the last blue point do not represent valid behaviours, because some probabilities associated with these points are negative. Taking into account only the points that represent valid probability distributions, one can readily see that the errors associated with the line $X + Y = 1.01$ are noticeably greater than the errors associated with lines $X + Y = 1$ and $X + Y = 0.99$. This leads me to conjecture that inequality 3.48 is tight in the affine subspace spanned by the behaviours 3.35-3.37.

Figure 14 – Optimization error for behaviours satisfying $X + Y = 1 + \epsilon$. Blue points correspond to behaviours inside the proposed boundary ($\epsilon = -0.01$); orange points correspond to behaviours at the proposed boundary ($\epsilon = 0$); Green points correspond to behaviours outside the proposed boundary ($\epsilon = +0.01$). The first and last green points as well as the last blue point do not correspond to valid behaviours, because some probabilities are negative. Excluding these points, we see that there is a noticeable increase in the optimization error when we go from inside or at the proposed boundary to behaviours outside it. This is numerical evidence that inequality 3.48 is indeed the bilocal boundary in the affine subspace spanned by distributions 3.35-3.37.

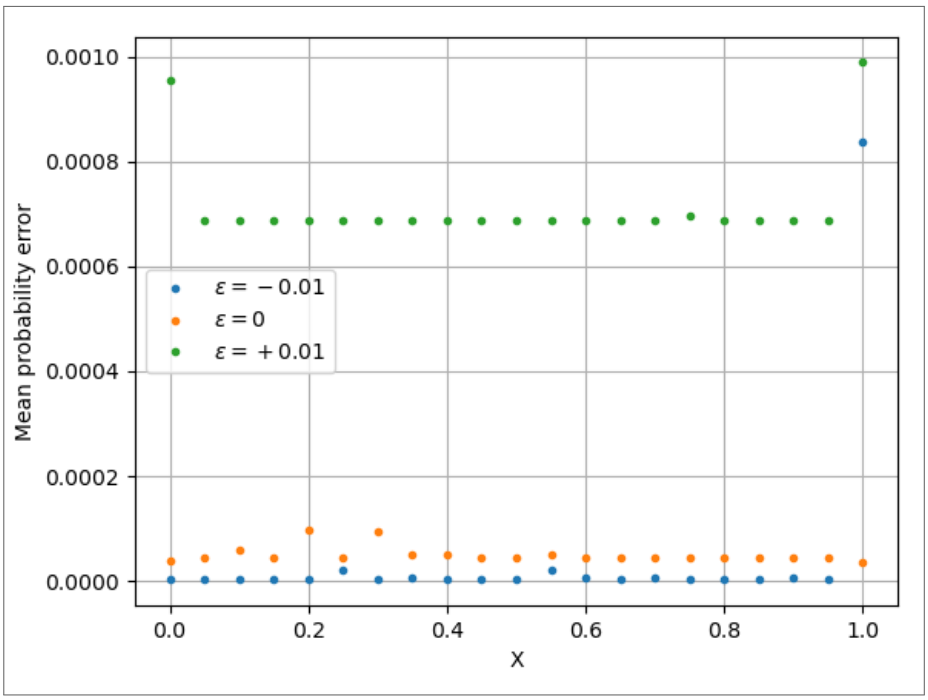

Source: personal archive

I hope this last example has shown how the solutions of problem 3.5 in 2-dimensional sets can be a valuable asset in the study of non-locality in network scenarios.

4 CONCLUSION AND PERSPECTIVES

Numerical solutions of problem 3.5 were used to shed light on the following problems in network non-locality:

i) determination of explicit local models for given behaviours (section 3.3)

ii) estimation of visibility thresholds for network locality (section 3.3)

iii) estimation of the boundary of the network local set in 2-dimensional slices of the probability space (section 3.4)

The first area where future work could be done is in trying to improve the execution time and accuracy of the numerical routine. In the implementation used to generate figures 8, 9 and 12, each time the solver attempts to find a local model, the initial guess is completely random. So if an acceptable model was found for one point, this achievement is not taken into account when investigating close points. Doing this could help expedite calculations and also reduce the probability of failure when trying to find a model for a point which is network local. In certain affine subspaces, symmetry could also be an important factor. For example, in the subspace of figure 9, the symmetries $I \to -I$ and $J \to -J$ correspond to simple relabelings of outputs and inputs. So there is actually no need to employ computing power in more than one quadrant.

An interesting issue is the matter of cardinality reduction in the hidden variables. As we saw in section 3.3, the behaviour obtained by the GHZ distribution mixed with the uniform distribution with visibility $v = 1/3$ could be obtained with cardinalities $c_\alpha = 2$, $c_\beta = 2$ and $c_\gamma = 3$, although the upper bound provided by equation 3.1 is $c_\alpha = c_\beta = c_\gamma = 6$. This cardinality reduction is not always possible, however. Consider the so called W distribution, inspired by the well known W quantum state:

$$p_W(a,b,c) = \begin{cases} 1/3, & \text{if } a+b+c=1 \\ 0, & \text{otherwise} \end{cases} \tag{4.1}$$

The behaviour obtained by mixing this distribution with the uniform distribution with visibility $v = 1/2$ seems to be bilocal (mean error less than 2×10^{-6}), but for this, the full alphabet of 6 values for α, β and γ seems to be necessary. Why is it that some probability

distributions allow for cardinality reduction, while others do not? An investigation of this question could provide some insight into network non-locality.

Another possible avenue for further research is to try to prove that inequality 3.48 is indeed tight in the affine subspace spanned by the probability distributions 3.35-3.37. If this conjecture turns out to be true, how do the parameters X and Y relate to the probabilities $p(a, b, c|x, y, z)$? Are there network quantum behaviours that violate inequality 3.48? The answer to these questions could lead to a better understanding of non-locality in the bilocal network, perhaps even to a new Bell-like inequality applicable to the bilocal scenario.

Concerning the triangle scenario with no inputs, it might be interesting to study 2-dimensional sets as we did for the bilocal network. Detailed analysis of 3-dimensional affine subspaces are more computationally demanding, but could provide even more insight since it is still possible to make visual representations of such sets.

Finally, it is worth developing an analogous numerical tool for quantum behaviours. The solver would then try to optimize over the density matrix of each source and the POVM matrices of each party. Unlike the situation of network local behaviours, where the cardinality of hidden variables is bounded, network quantum sets are more challenging, because there is no result limiting the dimensions of the Hilbert spaces for the quantum states distributed by the sources in network scenarios. Therefore, it is not possible to estimate the boundary of the quantum set in the same way done in section 3.4 for the local set, because the algorithm would have to assume a dimension for the Hilbert spaces of the sources that might not be enough to replicate all quantum behaviours. However, the ability to obtain an explicit realization of some quantum behaviours is certainly desirable when studying network non-locality, even if this is not possible in all cases.

BIBLIOGRAPHY

ASPECT, A.; DALIBARD, J.; ROGER, G. Experimental test of bell's inequalities using time-varying analyzers. *Phys. Rev. Lett.*, American Physical Society, v. 49, p. 1804–1807, Dec 1982. Available at: <https://link.aps.org/doi/10.1103/PhysRevLett.49.1804>.

BAGGOTT, J. E. *Beyond measure: Modern physics, philosophy, and the meaning of quantum theory*. [S.l.]: Oxford University Press on Demand, 2004.

BELL, J. S. On the einstein podolsky rosen paradox. *Physics Physique Fizika*, APS, v. 1, n. 3, p. 195, 1964.

BOHM, D. *Quantum Theory*. Dover Publications, 1951. (Dover Books on Physics Series). ISBN 9780486659695. Available at: <https://books.google.com.br/books?id=9DWim3RhymsC>.

BRANCIARD, C.; GISIN, N.; PIRONIO, S. Characterizing the nonlocal correlations created via entanglement swapping. *Physical review letters*, APS, v. 104, n. 17, p. 170401, 2010.

BRANCIARD, C.; ROSSET, D.; GISIN, N.; PIRONIO, S. Bilocal versus nonbilocal correlations in entanglement-swapping experiments. *Physical Review A*, APS, v. 85, n. 3, p. 032119, 2012.

BRUNNER, N.; CAVALCANTI, D.; PIRONIO, S.; SCARANI, V.; WEHNER, S. Bell nonlocality. *Reviews of Modern Physics*, APS, v. 86, n. 2, p. 419, 2014.

BYRD, R.; HRIBAR, M.; NOCEDAL, J. An interior point algorithm for large-scale nonlinear programming. *SIAM Journal on Optimization*, Society for Industrial and Applied Mathematics Publications, v. 9, n. 4, p. 877–900, Sep. 1999. ISSN 1052-6234.

CIREL'SON, B. Quantum generalizations of Bell's inequality. *Letters in Mathematical Physics*, v. 4, n. 2, p. 93–100, Mar. 1980.

CLAUSER, J. F.; HORNE, M. A.; SHIMONY, A.; HOLT, R. A. Proposed experiment to test local hidden-variable theories. *Phys. Rev. Lett.*, American Physical Society, v. 23, p. 880–884, Oct 1969. Available at: <https://link.aps.org/doi/10.1103/PhysRevLett.23.880>.

COLLINS, D.; GISIN, N. A relevant two qubit bell inequality inequivalent to the CHSH inequality. *Journal of Physics A: Mathematical and General*, IOP Publishing, v. 37, n. 5, p. 1775–1787, jan 2004. Available at: <https://doi.org/10.1088/0305-4470/37/5/021>.

EINSTEIN, A.; BORN, M.; BORN, H.; BORN, I. *The Born-Einstein Letters: Correspondence Between Albert Einstein and Max and Hedwig Born from 1916-1955, with Commentaries by Max Born*. Macmillan, 1971. ISBN 9780333112670. Available at: <https://books.google.com.br/books?id=HvZAAQAAIAAJ>.

EINSTEIN, A.; PODOLSKY, B.; ROSEN, N. Can quantum-mechanical description of physical reality be considered complete? *Phys. Rev.*, American Physical Society, v. 47, p. 777–780, May 1935. Available at: <https://link.aps.org/doi/10.1103/PhysRev.47.777>.

EKERT, A. K. Quantum cryptography based on bell's theorem. *Phys. Rev. Lett.*, American Physical Society, v. 67, p. 661–663, Aug 1991. Available at: <https://link.aps.org/doi/10.1103/PhysRevLett.67.661>.

FINE, A. Hidden variables, joint probability, and the bell inequalities. *Phys. Rev. Lett.*, American Physical Society, v. 48, p. 291–295, Feb 1982. Available at: <https://link.aps.org/doi/10.1103/PhysRevLett.48.291>.

FREEDMAN, S. J.; CLAUSER, J. F. Experimental test of local hidden-variable theories. *Phys. Rev. Lett.*, American Physical Society, v. 28, p. 938–941, Apr 1972. Available at: <https://link.aps.org/doi/10.1103/PhysRevLett.28.938>.

FRITZ, T. Beyond bell's theorem: correlation scenarios. *New Journal of Physics*, IOP Publishing, v. 14, n. 10, p. 103001, 2012.

GIUSTINA, M.; VERSTEEGH, M. A. M.; WENGEROWSKY, S.; HANDSTEINER, J.; HOCHRAINER, A.; PHELAN, K.; STEINLECHNER, F.; KOFLER, J.; LARSSON, J.-A.; ABELLÁN, C.; AMAYA, W.; PRUNERI, V.; MITCHELL, M. W.; BEYER, J.; GERRITS, T.; LITA, A. E.; SHALM, L. K.; NAM, S. W.; SCHEIDL, T.; URSIN, R.; WITTMANN, B.; ZEILINGER, A. Significant-loophole-free test of bell's theorem with entangled photons. *Phys. Rev. Lett.*, American Physical Society, v. 115, p. 250401, Dec 2015. Available at: <https://link.aps.org/doi/10.1103/PhysRevLett.115.250401>.

GREENBERGER, D. M.; HORNE, M. A.; SHIMONY, A.; ZEILINGER, A. Bell's theorem without inequalities. *American Journal of Physics*, v. 58, n. 12, p. 1131–1143, 1990. Available at: <https://doi.org/10.1119/1.16243>.

HENSEN, B.; BERNIEN, H.; DRéAU, A. E.; REISERER, A.; KALB, N.; BLOK, M. S.; RUITENBERG, J.; VERMEULEN, R. F. L.; SCHOUTEN, R. N.; ABELLáN, C.; AMAYA, W.; PRUNERI, V.; MITCHELL, M. W.; MARKHAM, M.; TWITCHEN, D. J.; ELKOUSS, D.; WEHNER, S.; TAMINIAU, T. H.; HANSON, R. Loophole-free Bell inequality violation using electron spins separated by 1.3 kilometres. *Nature*, Nature Publishing Group, a division of Macmillan Publishers Limited. All Rights Reserved., v. 526, n. 7575, p. 682–686, Oct. 2015. ISSN 0028-0836. Available at: <http://dx.doi.org/10.1038/nature15759>.

NAVASCUÉS, M.; WOLFE, E. The inflation technique completely solves the causal compatibility problem. *Journal of Causal Inference*, De Gruyter, v. 8, n. 1, p. 70–91, 2020.

NIELSEN, M.; CHUANG, I. *Quantum Computation and Quantum Information*. Cambridge University Press, 2000. (Cambridge Series on Information and the Natural Sciences). ISBN 9780521635035. Available at: <https://books.google.com.br/books?id=65FqEKQOfP8C>.

RENOU, M.-O.; BÄUMER, E.; BOREIRI, S.; BRUNNER, N.; GISIN, N.; BEIGI, S. Genuine quantum nonlocality in the triangle network. *Physical review letters*, APS, v. 123, n. 14, p. 140401, 2019.

RENOU, M.-O.; WANG, Y.; BOREIRI, S.; BEIGI, S.; GISIN, N.; BRUNNER, N. Limits on correlations in networks for quantum and no-signaling resources. *Phys. Rev. Lett.*, American Physical Society, v. 123, p. 070403, Aug 2019. Available at: <https://link.aps.org/doi/10.1103/PhysRevLett.123.070403>.

ROSSET, D.; GISIN, N.; WOLFE, E. Universal bound on the cardinality of local hidden variables in networks. *arXiv preprint arXiv:1709.00707*, 2017.

SCARANI, V. *Bell nonlocality*. [S.l.]: Oxford Graduate Texts, 2019.

SHALM, L. K.; MEYER-SCOTT, E.; CHRISTENSEN, B. G.; BIERHORST, P.; WAYNE, M. A.; STEVENS, M. J.; GERRITS, T.; GLANCY, S.; HAMEL, D. R.; ALLMAN, M. S.; COAKLEY, K. J.; DYER, S. D.; HODGE, C.; LITA, A. E.; VERMA, V. B.; LAMBROCCO, C.; TORTORICI, E.; MIGDALL, A. L.; ZHANG, Y.; KUMOR, D. R.; FARR, W. H.; MARSILI, F.; SHAW, M. D.; STERN, J. A.; ABELLÁN, C.; AMAYA, W.; PRUNERI, V.; JENNEWEIN, T.; MITCHELL, M. W.; KWIAT, P. G.; BIENFANG, J. C.; MIRIN, R. P.; KNILL, E.; NAM, S. W. Strong loophole-free test of local realism. *Phys. Rev. Lett.*, American Physical Society, v. 115, p. 250402, Dec 2015. Available at: <https://link.aps.org/doi/10.1103/PhysRevLett.115.250402>.

ŠUPIĆ, I.; BOWLES, J. Self-testing of quantum systems: a review. *Quantum*, Verein zur Förderung des Open Access Publizierens in den Quantenwissenschaften, v. 4, p. 337, Sep. 2020. ISSN 2521-327X. Available at: <https://doi.org/10.22331/q-2020-09-30-337>.

TAVAKOLI, A.; POZAS-KERSTJENS, A.; LUO, M.-X.; RENOU, M.-O. Bell nonlocality in networks. *arXiv preprint arXiv:2104.10700*, 2021.

VIRTANEN, P.; GOMMERS, R.; OLIPHANT, T. E.; HABERLAND, M.; REDDY, T.; COURNAPEAU, D.; BUROVSKI, E.; PETERSON, P.; WECKESSER, W.; BRIGHT, J.; van der Walt, S. J.; BRETT, M.; WILSON, J.; MILLMAN, K. J.; MAYOROV, N.; NELSON, A. R. J.; JONES, E.; KERN, R.; LARSON, E.; CAREY, C. J.; POLAT, İ.; FENG, Y.; MOORE, E. W.; VanderPlas, J.; LAXALDE, D.; PERKTOLD, J.; CIMRMAN, R.; HENRIKSEN, I.; QUINTERO, E. A.; HARRIS, C. R.; ARCHIBALD, A. M.; RIBEIRO, A. H.; PEDREGOSA, F.; van Mulbregt, P.; SciPy 1.0 Contributors. SciPy 1.0: Fundamental Algorithms for Scientific Computing in Python. *Nature Methods*, v. 17, p. 261–272, 2020.

WOLFE, E.; SPEKKENS, R. W.; FRITZ, T. The inflation technique for causal inference with latent variables. *Journal of Causal Inference*, De Gruyter, v. 7, n. 2, 2019.

ZIEGLER, G. *Lectures on Polytopes*. Springer New York, 2012. (Graduate Texts in Mathematics). ISBN 9780387943657. Available at: <https://books.google.com.br/books?id=xd25TXSSUcgC>.